Wu YW (6 人略) Tsutsui H (1 人略)	Heterogeneous reduction of myocardial oxidative metabolism in patients with ischemic and dilated cardiomyopathy using C-11 acetate PET	Circ J	72	786-792	2008
Makita N (14 人略) Tsutsui H (3 人略)	The E1784K mutation in SCN5A is associated with mixed clinical phenotype of type 3 long QT syndrome	J Clin Invest	118	2219-2229	2008
[室原 豊明] Inden Y Ito R (9 人略) Murohara T	Combined assessment of left ventricular dyssynchrony and contractility by speckled tracking strain imaging: A novel index for predicting responders to cardiac resynchronization therapy.	Heart Rhythm.	7	655-661	2010
Shimano M Ouchi N (3 人略) Murohara T Walsh K	Adiponectin deficiency exacerbates cardiac dysfunction following pressure overload through disruption of an AMPK-dependent angiogenic response.	J. Mol. Cell. Cardiol.	49	210-220	2010
Kondo K Shibata R (7 人略) Murohara T	Impact of a Single Intracoronary Administration of Adiponectin on Myocardial Ischemia/Reperfusion Injury in a Pig Model.	Circ. Cardiovasc. Interv.	3	166-173	2010
Morikawa S Sone T (7人略) Murohara T	Renal protective effects and the prevention of contrast-induced nephropathy by atrial natriuretic peptide.	J. Am. Coll. Cardiol.	53	1040-1046	2009
Unno K Shibata R (8人略) Murohara T	Adiponectin acts as a positive indicator of left ventricular diastolic dysfunction in patients with hypertrophic cardiomyopathy.	Heart		in press	2009
Numaguchi Y Ishii M (5人略) Murohara T	Ablation of Angiotensin IV Receptor Attenuates Hypofibrinolysis via PAI-1 Downregulation and Reduces Occlusive Arterial Thrombosis.	Arterioscler. Thromb. Vasc. Biol.	29	2102-2108	2009

Kitamura T Asai N (9 人略) Murohara T Takahashi M	Regulation of VEGF-mediated angiogenesis by the Akt/PKB substrate Girdin	Nat. Cell Biol	10	329-337	2008
Sugiura T Kondo T (7 人略) Murohara T	Nifedipine improves endothelial function : role of endothelial progenitor cell	Hypertension	52	491-498	2008
Li P Kondo T (4 人略) Murohara T	Role of bradykinin, nitric oxide and angiotensin II type 2 receptor in imidapril-induced angiogenesis	Hypertension	51	252-258	2008
[浅沼 博司] Takahama H Asanuma H (5 人略) Asakura M Takashima S Minamino T (2 人略) Kitakaze M	Histamine H_2 receptor blocker ameliorates development of heart failure in dogs independently of・・・adrenergic receptor blockade	Basic Res Cardiol	105	787-794	2010
Asanuma H Kitakaze M	Hypothetical mechanism of the improvement by adaptive servo-ventilation of the pathophysiology of heart failure associated with sleep-disordered breathing..	Circ J	74	2056-2057	2010
Sasaki H Asanuma H (5 人略) Asakura M (1 人略) Minamino T Takashima S (4 人略) Kitakaze M	Metformin prevents progression of heart failure in dogs: role of AMP-activated protein kinase	Circulation	119	2568-2577	2009
Takahama H Minamino T Asanuma H (7 人略) Asakura M (1 人略) Takashima S (3 人略) Kitakaze M	Prolonged targeting of ischemic/reperfused myocardium by liposomal adenosine augments cardioprotection in rats	J Am Coll Cardiol	53	709-717	2009

Asai M (1 人略) Minamino T Asanuma H (5 人略) Asakura M, Takashima S (1 人略) Kitakaze M	PKA rapidly enhances proteasome assembly and activity in in vivo canine hearts	Journal of molecular and cellular cardiology.	46	452-462	2009
Asanuma H Kitakaze M	Adiponectin is an Important Novel Therapeutic Target in Acute Decompensated Heart Failure - Effect of Carperitide on Plasma Adiponectin Levels -	Circ J	73	2206-2207	2009
Ohara T Kim J Asakura M Asanuma H (5 人略) Kitakaze M	Plasma adiponectin is associated with plasma brain natriuretic peptide and cardiac function in healthy subjects	Hypertens Res	31	825-831	2008
Fujita M Asakura M (4 人略) Asanuma H (6 人略) Kitakaze M	Activation of ecto-5'-nucleotidase in the blood and hearts of patients with chronic heart failure	Journal of Cardiac Failure	14	426-430	2008
[古川 秀比古] Min K Asakura M (7 人略) Asanuma H (1 人略) Minamino T (5 人略) Furukawa H (1 人略) Takashima S (1 人略) Kitakaze M	Identification of genes related to heart failure using global gene expression profiling of human failing myocardium	Biochem. Biophys. Res. Commun.		Feb. 17 [Epub ahead of print]	2009
Nakayama-Hamada M Suzuki A Furukawa H Yamada R Yamamoto K	Citrullinated fibrinogen inhibits thrombin-catalysed fibrin polymerization	Journal of biochemistry	144	393-398	2008

Left Atrial Volume Combined With Atrial Pump Function Identifies Hypertensive Patients With a History of Paroxysmal Atrial Fibrillation

Norihisa Toh, Hideaki Kanzaki, Satoshi Nakatani, Takahiro Ohara, Jiyoong Kim, Kengo F. Kusano, Kazuhiko Hashimura, Tohru Ohe, Hiroshi Ito, Masafumi Kitakaze

Abstract—Identifying patients at high risk for the occurrence of atrial fibrillation is one means by which subsequent thromboembolic complications may be prevented. Left atrial enlargement is associated with progression of atrial remodeling, which is a substrate for atrial fibrillation, but impaired atrial pump function is also another aspect of the remodeling. Our objective was to differentiate patients with a history of paroxysmal atrial fibrillation using echocardiography. We studied 280 hypertensive patients (age: 66±7 years; left ventricular ejection fraction: 65±8%), including 140 consecutive patients with paroxysmal atrial fibrillation and 140 age- and sex-matched control subjects. Left atrial volume was measured using the modified Simpson method at both left ventricular end systole and preatrial contraction and was indexed to body surface area. Peak late-diastolic mitral annular velocity was measured during atrial contraction using pulsed tissue Doppler imaging as an atrial pump function. Left atrial volume index measured at left ventricular end systole had a 74% diagnostic accuracy and a 71% positive predictive value for identifying patients with paroxysmal atrial fibrillation; these values for the ratio of left atrial volume index at left ventricular end systole to the peak late-diastolic mitral annular velocity were 82% and 81%, respectively, and those for the ratio of left atrial volume index at preatrial contraction to the peak late-diastolic mitral annular velocity were 86% and 90%, respectively. In conclusion, left atrial size combined with atrial pump function enabled a more accurate diagnosis of a history of paroxysmal atrial fibrillation than conventional parameters. (***Hypertension.* 2010;55:1150-1156.**)

Key Words: hypertension ■ echocardiography ■ atrial fibrillation ■ left atrium ■ remodeling

Atrial fibrillation (AF) is not generally life threatening but is considered to be the most common cause of ischemic stroke, which often yields serious complications because of acute occlusion of intracranial arteries without collateral circulation. The incidence of stroke is increased by ≈5-fold in the presence of nonvalvular AF.[1–5] Moreover, recent studies have demonstrated that stroke risk is no less in patients with paroxysmal AF (PAF) than in those with persistent AF.[6] Therefore, it is crucial to identify patients who have PAF in order to prevent subsequent thromboembolic complications, especially in patients with hypertension, which is a major etiologic factor associated with both AF and stroke.[7–9]

Left atrial (LA) enlargement associated with the progression of atrial structural remodeling plays a key role in the initiation and maintenance of AF.[10,11] The most recent recommendations for echocardiographic chamber quantification indicate that LA volume (LAV) provides an accurate measurement of asymmetrical remodeling of the LA chamber.[12] LAV is increased in patients with PAF[13] and is also an important predictor of cardiovascular outcome, including the occurrence of AF,[14] supporting the concept that LAV is a hallmark of atrial remodeling.

In patients with PAF, Doppler transmitral flow velocity and tissue Doppler imaging (TDI)–derived mitral annulus velocity during atrial contraction, which are considered to reflect atrial pump function,[15–20] have been reported to be decreased compared with those in control subjects.[13,16,21] According to the Frank-Starling law, atrial pump function is also enhanced with an increase in LAV; however, excessive LA enlargement leads to atrial dysfunction.[22,23] Accordingly, we hypothesized that adding information on atrial pump function may provide a better marker of atrial remodeling.

In the present study, we aimed to differentiate patients with a history of PAF among those with hypertension more accurately by means of LAV combined with atrial pump function.

Methods

Study Population

Patients referred to our laboratory were classified into the PAF group if they met the following criteria: (1) ≥1 episode of self-terminating

Received June 18, 2009; first decision July 6, 2009; revision accepted March 8, 2010.

From the Cardiovascular Division of Medicine (N.T., H.K., S.N., T.O., J.K., K.H., M.K.), National Cardiovascular Center, Osaka, Japan; Department of Cardiovascular Medicine (K.F.K., H.I.), Okayama University Graduate School of Medicine, Dentistry, and Pharmaceutical Sciences, Okayama, Japan; Department of Cardiology (T.O.), Sakakibara Heart Institute of Okayama, Okayama, Japan.

Correspondence to Hideaki Kanzaki, Cardiovascular Division of Medicine, National Cardiovascular Center, 5-7-1 Fujishiro-dai, Suita, Osaka 565-8565, Japan. E-mail kanzakih@hsp.ncvc.go.jp

***Hypertension* is available at http://hyper.ahajournals.org** **DOI: 10.1161/HYPERTENSIONAHA.109.137760**

PAF documented by a 12-lead ECG, 24-hour Holter monitoring, or continuous monitoring during hospitalization without taking any antiarrhythmic drugs and having been free from arrhythmic episodes for >1 week before undergoing echocardiography; (2) hypertension (systolic blood pressure ≥140 mm Hg and/or diastolic blood pressure ≥90 mm Hg or treatment for hypertension); (3) less than moderate mitral regurgitation; (4) sinus rhythm during echocardiography; (5) no medical history of other arrhythmias (including persistent AF), valvular heart disease (including mitral annular calcification), heart failure, ischemic heart disease, cardiomyopathy, cardiac surgery, thyroid disease, or pulmonary disease; and (6) age between 40 and 80 years.

Control subjects were recruited from a clinical health examination in Arita, Japan. All of the attendees underwent a formal medical history interview, ECG, and physical and laboratory examinations. Blood pressure was measured at each of ≥2 visits to the office, and the average of ≥2 seated blood pressures was used according to established recommendations.[24] Of the attendees who also underwent echocardiography, age- and sex-matched subjects who met criteria 2 through 6 were classified as the control group. The study was approved by the institutional review board, and the study was conducted in accordance with the ethical principles of the Declaration of Helsinki. All of the subjects provided informed consent.

Echocardiography

All of the echocardiographic studies were performed with either a Vivid 7 Dimension (GE Healthcare) or Aplio XV (Toshiba Medical Systems) ultrasound system. Cardiac chamber size, left ventricular (LV) ejection fraction (LVEF), LV mass, and LA dimension were evaluated according to the recommendations of the American Society of Echocardiography.[12] LAV was measured using the biplane modified Simpson's method at the ventricular end-systolic frame just before the mitral valve opening from apical 4- and 2-chamber views. Strictly speaking, however, LA does not contract from the size of LAV at ventricular end systole. Thus, preatrial contraction LAV (LAV_{preA}) was also obtained from the last frame just before mitral valve reopening. Active LA emptying fraction (active LAEF) was calculated by the following formula: $(LAV_{preA}-LAV_{min})/LAV_{preA}\times100\%$, where LAV_{min} is the minimal LAV at atrial end systole. All of the LAVs were indexed to body surface area as LAVi, $LAVi_{preA}$, and $LAVi_{min}$, respectively. LV mass was also indexed to body surface area (LV mass index). LV hypertrophy was defined as LV mass index >104 g/m^2 in women and >116 g/m^2 in men.[25]

The sample volume of pulsed-wave Doppler imaging was placed at the tip level of the mitral leaflets in the apical 4-chamber view. Then the peak mitral inflow early diastolic and atrial filling (E and A) velocities and the E-wave deceleration time were obtained. The sample volume of the pulsed TDI was placed at the septal and lateral margins of the mitral annulus. Peak early and late-diastolic mitral annular velocities were measured, and then the average values of septal and lateral velocities were used as Ea and Aa, respectively. E/Ea was calculated as a surrogate for the LV filling pressure.[26]

Statistical Analysis

Data are expressed as mean±SD. An ANOVA was performed to test for statistically significant differences between 2 unpaired mean values, and categorical data and percentage frequencies were analyzed by the χ^2 test. Correlations were determined with Pearson product moment correlation analysis. Receiver operating characteristic (ROC) curves were constructed to determine the optimal sensitivity and specificity. The area under the curve (AUC) was calculated to assess the overall performance of various variables for the detection of PAF. Univariate and multivariate logistic regression analyses were performed to characterize diagnostic factors of a history of PAF. Variables considered included age, sex, body weight, LV hypertrophy, E/Ea, and diabetes mellitus. A scatter diagram was used to illustrate the relationship between LA size and LA pump function in each patient. A straight line was drawn passing through the origin to discriminate the best between the PAF and control groups, and another line was drawn to establish the boundary above which spots belonging to the PAF group existed. The slope indicates the ratio of LA size to LA pump function: the former corresponds to the optimal cutoff value from the ROC analysis and the latter is the minimum of the ratios of the PAF group. Most statistical tests were performed with SPSS version 12.0 (SPSS Inc). The calculation and comparison of AUC values and the logistic regression analyses were performed with Stata SE version 8.2 (Stata Corp). A P value <0.05 was considered to be statistically significant. The statistical power of the present study was finally calculated.

Forty subjects were randomly selected from each group and analyzed blindly by 2 authors (N.T. and H.K.) to assess reproducibility. The interobserver and intraobserver variabilities were, respectively, 4.0% and 3.8% for LAV, 4.2% and 4.2% for LAV_{preA}, 12.3% and 9.9% for LAV_{min}, 4.4% and 4.1% for peak A velocity, 3.6% and 3.5% for septal Aa, and 4.0% and 3.7% for lateral Aa.

Table 1. Clinical Characteristics of the Study Population

Variable	Control Group (n=140)	PAF Group (n=140)
Age, y	66±7	66±8
Women, %	47	47
Height, cm	158±9	160±10
Weight, kg	58±10	60±10
Body surface area, m^2	1.59±0.17	1.60±0.26
Body mass index, kg/m^2	23.2±3.3	23.6±3.0
Systolic blood pressure, mm Hg	140±18	137±16
Diastolic blood pressure, mm Hg	82±10	80±11
Diabetes mellitus, %	17	21
Hyperlipidemia, %	46	47
Smoking, %	31	23
Concomitant cardiovascular therapies		
ACE inhibitors, %	7	5
ARBs, %	30	32
β-Blockers, %	18	27
Calcium channel blockers, %	32	37

Values are expressed as mean±SD unless otherwise specified. ACE indicates angiotensin-converting enzyme; ARB, angiotensin II receptor blockers. No significant differences were found between groups.

Results

Clinical and Echocardiographic Characteristics

A total of 280 subjects with hypertension (mean age: 66±7 years; range: 40 to 80 years; 148 men; LVEF: 65±8%) were enrolled in the present study. There were no significant differences in clinical parameters or the use of antihypertensive drugs between the 140 control and 140 PAF subjects (Table 1). The median time interval between the first PAF episode and this examination was 2.0 years (25th to 75th percentile: 0.2 to 7.0 years), and 62% of the patients with PAF were symptomatic. Echocardiographic characteristics are depicted in Table 2. No significant group differences were found for the following parameters: LV end-diastolic diameter, LV end-systolic diameter, and LVEF. LV mass index, LA dimension, and indices related to the LAV were significantly increased in the PAF group compared with those in the control group, whereas active LAEF was decreased in the PAF group. The prevalences of LV hypertrophy were 45% in the PAF group (37 women and 25 men) and 28% in the control group (18 women and 21 men). The E-wave decel-

Table 2. Echocardiographic Characteristics of the Study Population

Variable	Control Group (n=140)	PAF Group (n=140)	*P*
LV end-diastolic dimension, mm	47±5	46±5	0.114
LV end-systolic dimension, mm	28±5	28±5	0.445
LVEF, %	65±8	65±8	0.839
LV mass index, g/m^2	100±20	112±27	<0.001
LA dimension, mm	38±5	43±5	<0.001
LAVi, ml/m^2	30±7	42±12	<0.001
$LAVi_{preA}$, ml/m^2	21±6	32±10	<0.001
$LAVi_{min}$, ml/m^2	14±4	25±10	<0.001
Active LAEF, %	34±8	23±10	<0.001
Peak E velocity, cm/s	64±15	70±19	0.007
Peak A velocity, cm/s	80±18	67±21	<0.001
E/A	0.85±0.24	1.18±0.67	<0.001
E-wave deceleration time, ms	233±44	224±49	0.069
Ea, cm/s	7.5±1.9	6.8±1.9	<0.001
Aa, cm/s	11.1±2.3	7.7±2.6	<0.001
E/Ea	9.0±2.5	11.1±4.3	<0.001
LAVi/A, mL · m^{-2}/cm · s^{-1}	0.39±0.11	0.72±0.41	<0.001
LAVi/Aa, mL · m^{-2}/cm · s^{-1}	2.9±1.0	6.8±5.1	<0.001
$LAVi_{preA}$/active LAEF	0.64±0.28	1.96±2.23	<0.001
$LAVi_{preA}$/A, mL · m^{-2}/cm · s^{-1}	0.27±0.08	0.55±0.36	<0.001
$LAVi_{preA}$/Aa, mL · m^{-2}/cm · s^{-1}	1.9±0.4	5.3±4.3	<0.001

Values are expressed as mean±SD.

eration time was comparable, but peak E velocity was significantly greater, and peak A velocity was less in the PAF group than in the control group. The Ea and Aa were lower in the PAF group than in the control group. E/Ea was greater in the PAF group than in the control group.

The following correlations were found: (1) LAVi and $LAVi_{preA}$ were correlated with E/Ea (LAVi: r=0.418, P<0.001; $LAVi_{preA}$: r=0.416, P<0.001); (2) LAVi and $LAVi_{preA}$ were correlated with LV mass index (LAVi: r=0.440, P<0.001; $LAVi_{preA}$: r=0.459, P<0.001); (3) LAVi was strongly correlated with the $LAVi_{preA}$ (r=0.916; P<0.001); (4) Aa was correlated well with active LAEF (r=0.755; P<0.001) and this correlation was still observed in patients with severely enlarged LA (r=0.775; P<0.001), which is defined as LAVi >40 mL/m^2 in the recommendations[12]; and (5) LAVi/Aa and $LAVi_{preA}$/Aa were correlated with the time interval between the first PAF episode and this examination (LAVi/Aa: r=0.267, P=0.012; $LAVi_{preA}$/Aa: r=0.275, P=0.009).

Echocardiographic Detection of PAF Among Hypertensive Patients

Various parameters, listed in Table 3, were examined using ROC analysis. $LAVi_{preA}$/Aa was best for detecting patients with a history of PAF considering the AUC. The AUC of $LAVi_{preA}$/Aa was statistically greater than those of the $LAVi_{preA}$/A, $LAVi_{preA}$/active LAEF, LAVi/Aa, and LAVi values (P=0.024, P=0.003, P<0.001, and P<0.001, respectively). Although the statistical power calculated was 76% because of the limited number of subjects, statistically significant differences were found between the $LAVi_{preA}$/Aa ratio and other parameters. The ROC curves for the $LAVi_{preA}$/Aa, LAVi/Aa, LAVi, and LA dimension are shown in Figure 1.

Table 3. AUCs for Echocardiographic Variables

Variable	AUC	SE	95% CI
LA dimension	0.733	0.030	0.675 to 0.791
LAVi	0.820	0.024	0.772 to 0.868
$LAVi_{preA}$	0.861	0.022	0.819 to 0.904
LAVi/A	0.852	0.023	0.807 to 0.898
LAVi/Aa	0.884	0.019	0.847 to 0.922
$LAVi_{preA}$/active LAEF	0.893	0.019	0.856 to 0.930
$LAVi_{preA}$/A	0.888	0.020	0.849 to 0.927
$LAVi_{preA}$/Aa	0.927	0.015	0.897 to 0.956

The sensitivity, specificity, diagnostic accuracy, and positive predictive value for the detection of PAF were determined with an optimal cutoff value according to the ROC analysis, as shown in Table 4. Diagnostic accuracy and positive predictive value of the $LAVi_{preA}$/Aa ratio at the cutoff value of >2.7 mL · m^{-2}/cm · s^{-1} were clearly superior to those of the LAVi of >32.0 mL/m^2.

From the results of univariate analysis for age, sex, body weight, LV hypertrophy, E/Ea, and diabetes mellitus, LV hypertrophy (odds ratio: 2.059 [95% CI: 1.251 to 3.386]; P<0.001) and E/Ea (odds ratio: 1.205 [95% CI: 1.108 to 1.309]; P<0.001) were considered as significant covariates. However, multivariate analysis demonstrated that the $LAVi_{preA}$/Aa ratio was the single significant factor of a history of PAF (odds ratio: 11.786 [95% CI: 6.178 to 22.483]; P<0.001).

LA Size Against Atrial Pump Function

The relationship between LA size and atrial pump function in our population is illustrated in Figure 2. LA size and Aa showed an inverse correlation (LAVi: r=−0.503, P<0.001; $LAVi_{preA}$:

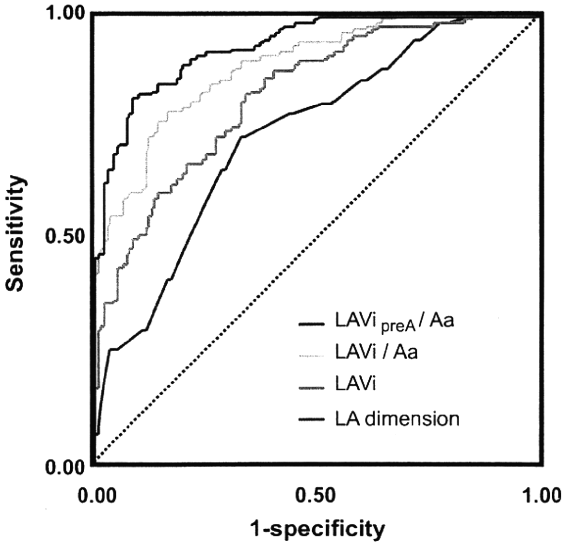

Figure 1. ROC curves for detecting PAF. Comparison of ROC curves for the $LAVi_{preA}$/Aa (red line), LAVi/Aa (yellow line), LAVi (green line), and LA dimension (blue line) values. The AUC values are listed in Table 3.

Table 4. Evaluation of Echocardiographic Parameters According to Sensitivity, Specificity, and Diagnostic Accuracy for Detection of PAF in Hypertensive Patients

Variable	Sensitivity, %	Specificity, %	Diagnostic Accuracy, %	PPV, %
LA dimension >41 mm	72	67	71	69
LAVi >32.0 mL/m^2	82	66	74	71
LAVi/A >0.50 mL · m^{-2}/cm · s^{-1}	75	87	81	85
LAVi/Aa >3.6 mL · m^{-2}/cm · s^{-1}	78	84	82	81
$LAVi_{preA}$/A >0.36 mL · m^{-2}/cm · s^{-1}	80	85	83	84
$LAVi_{preA}$/Aa >2.7 mL · m^{-2}/cm · s^{-1}	82	91	86	90

Values are expressed as percentage. PPV indicates positive predictive value.

$r=-0.458$, $P<0.001$). The PAF group is located disproportionately in the upper left part as compared with the control group. The black dotted lines discriminate best between the PAF and control groups, with slopes of 3.6 (the LAVi/Aa ratio=3.6 mL · m^{-2}/cm · s^{-1}) and 2.7 (the $LAVi_{preA}$/Aa ratio=2.7 mL · m^{-2}/cm · s^{-1}), respectively. The red dotted lines show the lower bound of the PAF group, with slopes of 2.3 and 1.9, respectively.

Discussion

The LA of hypertensive patients with PAF was characterized by further enlargement and impaired pump function as compared with that of hypertensive patients in whom PAF had never been documented. Thus, the ratio of $LAVi_{preA}$ to Aa was most powerful, and the ratio of LAVi to Aa was the next most powerful for differentiating hypertensive patients with a history of PAF.

LA Remodeling in Hypertension

LA size has been reported to serve as a surrogate measure of chronic LV diastolic dysfunction.[27] Hypertension induces an increase in LV wall stress, leading to increased wall thickness, myocyte hypertrophy, and myocardial fibrosis.[28,29] Impaired myocardial relaxation and increased LV diastolic stiffness can cause elevated LV diastolic filling pressure,[30] consistent with the increase in E/Ea. Moreover, long-standing hypertension results in interstitial fibrosis and arrhythmic substrate even in the LA.[31] In a large cohort study, increased LV mass and LA diameter were independently associated with the occurrence of AF in patients with hypertension.[32] Similarly, we found that LV mass index, E/Ea, and LAVi values were significantly increased in our hypertensive patients with PAF compared with those in hypertensive patients without PAF. In addition, LAVi showed a significant correlation with both LV mass index and E/Ea. These findings do not contradict the concept that the occurrence of PAF in hypertension is associated with LA remodeling as a consequence of LA overload because of elevated LV filling pressure.

The $LAVi_{preA}$/Aa and LAVi/Aa ratios showed a very modest but yet significant correlation with the time interval between the first PAF episode and this examination. LA remodeling is thought to progress according to not only the LA overload but also the duration of AF.[33] Thus, the indices that we proposed may be markers representing the degrees of progressive LA remodeling.

Frank-Starling Mechanism of LA Function

According to the Frank-Starling mechanism, contractile force of the ventricular myocardium is proportional to its initial length; this mechanism also applies to the LA myocardium.[22,23] LA pump function is enhanced in response to elevated LV filling pressure as long as the Frank-Starling mechanism holds. Within the range of compensation, therefore, the points in Figure 2 should range toward the upper right direction; in contrast, the points belonging to the PAF group are located in the upper left area. This disproportional distribution is also thought to demonstrate a shift of or a deviation from the Frank-Starling curves because of further progression of atrial remodeling in the PAF group. In addition, Figure 2 shows that patients with an LAVi/Aa ratio ≥2.3 mL · m^{-2}/cm · s^{-1}

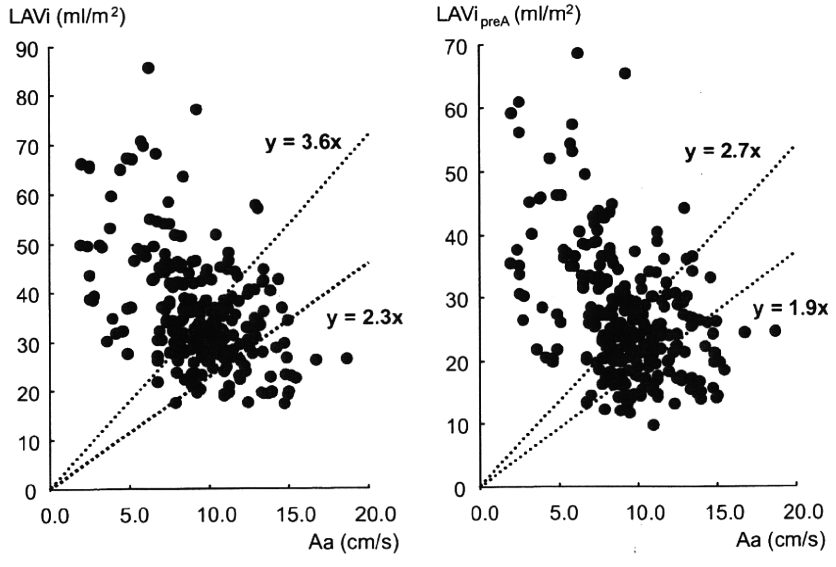

Figure 2. Relationship between LA size and pump function in patients with and without PAF. Scatter diagrams showing the distribution of plots of the LAVi against Aa values (left) and $LAVi_{preA}$ against Aa values (right). Red points indicate hypertensive patients with PAF, and blue points indicate hypertensive patients in whom PAF has never been documented. Patients with LAVi/Aa ratios >2.3 mL · m^{-2}/cm · s^{-1} or $LAVi_{preA}$/Aa ratios >1.9 mL · m^{-2}/cm · s^{-1} may have PAF.

or $LAVi_{preA}$/Aa ratio ≥ 1.9 mL · m^{-2}/cm · s^{-1} may potentially have a history of PAF.

Preload is originally reflected as the initial stretching of cardiac myocytes before contraction. Thus, when adding atrial function to LA size for assessing atrial remodeling, $LAVi_{preA}$ is thought to be physiologically more preferable to LA size than is LAVi. Therefore, it was a reasonable result that the $LAVi_{preA}$/Aa ratio showed better diagnostic ability than the LAVi/Aa ratio.

Measurement of Atrial Pump Function

Several past studies have demonstrated that Aa velocity correlates well with atrial contractile function and can be used as a rapid and accurate marker of atrial function.[16–20] Similar to results of these studies, Aa showed a significant correlation with active LAEF in our study, and the correlation of Aa with active LAEF also remained in patients with excessive LA enlargement.

The changes in flow velocity profile with different positions of the pulsed-wave Doppler sample volume may affect the diagnostic accuracy of the $LAVi_{preA}$/A ratio. Even slight changes in sample volume position can easily cause a decrease in peak A velocity.[34] In contrast, TDI-derived mitral annulus velocities are relatively independent of these problems.[35] Our results also show that Aa is a marker reflecting atrial pump function.

Lateral Aa is a favorable discrimination parameter because its amplitude is greater than that of septal Aa. However, the left lung often attenuates tissue Doppler signals from the lateral annulus margin. The mitral septal annulus motion is always parallel to the Doppler beam, and its measurements are certain. Septal Aa could, however, be influenced by right atrial pump function. In the present study, therefore, we used the average of the septal and lateral Aas.

Study Limitations

First, this was a cross-sectional study. To clarify whether the present index can predict future AF development or complications, further research must provide longitudinal assessments. Second, it is difficult to distinguish whether the impaired atrial pump function was attributed to LA remodeling or showed a recovery process after spontaneous conversion of AF. This issue does not concern the diagnosis of PAF, but it may slightly affect the cutoff value for detecting PAF. Third, atrial reservoir function was not examined in the present study. Some reports indicate that evaluating LA reservoir function using strain or strain rate is useful for the prediction of AF relapse after treatments.[36,37] Nevertheless, we chose to use pulsed TDI parameters for the following reasons: (1) measurement of strain or strain rate with high reproducibility or using the speckle tracking method requires a high-end ultrasound machine and special dedicated software, but pulsed TDI is available on almost all machines; (2) peak late-diastolic atrial strain rate during atrial contraction has been reported to be correlated well with Aa[38,39]; (3) speckle tracking software, which is used when measuring atrial strain or strain rate, is designed primarily for the LV and not the LA; and (4) atrial strain or strain rate reflects only regional function of the LA, and the position of regions of interest for assessing LA global pump function is still controversial, whereas Aa is a marker of atrial global function and has been validated by cardiac catheters.[17] We preferred this general technology because our goal was to make our method accessible. Fourth, we did not measure pulmonary venous flow for assessing LV diastolic function because obtaining an adequate signal for analysis has been reported to be difficult in all subjects.[40,41] Furthermore, a recent consensus statement recommends tissue Doppler velocities as a first-line echocardiographic diagnostic approach to LV diastolic dysfunction.[42] Fifth, obtaining an accurate time interval between the first PAF episode and the current examination was practically difficult because PAF is, by nature, an elusive disease, and the majority of PAF episodes are known to be asymptomatic.[43] Similarly, the first PAF episode in asymptomatic patients was noticed incidentally as an irregularly irregular rhythm during auscultation or palpitating arterial pulse and was confirmed using ECG at a monthly or biweekly consultation day; thus, the interval may be not accurate. Little information on the number and duration of PAF episodes was available in the present study. Finally, we cannot clearly state that self-terminating spontaneous AF was never present in hypertensive patients with PAF within 1 week of examination or in patients with hypertension alone; nonetheless, we addressed this concern by performing repeated 12-lead ECGs, 24-hour Holter monitoring, and strict medical interviews for the subjects of the study.

Perspectives

Our observations that the LA of hypertensive patients with PAF is characterized by dilatation and impaired pump function and that the ratio of LA size to pump function is useful for identifying patients with PAF have important public health and clinical implications. If the presence of PAF is suspected at the time of echocardiography, further examinations and careful monitoring (including repeated 24-hour or event-ECG Holter recording) may be considered. This is especially true for patients with multiple risk factors for stroke (eg, congestive heart failure, hypertension, age >75 years, diabetes mellitus, and previous stroke or transient ischemic attack). In other words, the present indices may be useful for recommending preventive therapy in high-risk patients, because clinicians can prevent the greater part of ischemic stroke from AF with anticoagulation therapy.[44] A recent report from the Framingham Heart Study proposed a risk score for the future development of AF, but echocardiographic parameters provided only slight improvement in the risk assessment score.[45] The measurements derived from the conventional M-mode method may have attenuated the benefits of echocardiography in the aforementioned study. We expect that the new marker presented here (LA size divided by atrial pump function) will improve risk classification in future prospective studies.

Acknowledgments

We thank the members of the Arita Cohort Studies Unit for their valuable assistance with patient investigations, as well as Yoshiyuki Sumita, Tetsuhiro Yamano, Haruhiko Abe, and Takuya Hasegawa for obtaining excellent echocardiographic data.

Sources of Funding

This study was supported by a grant from the Japan Heart Foundation.

Disclosures

None.

References

1. Fleqel KM, Shipley MJ, Rose G. Risk of stroke in non-rheumatic atrial fibrillation. *Lancet*. 1987;1:526–529.
2. Lévy S, Maarek M, Coumel P, Guize L, Lekieffre J, Medvedowsky JL, Sebaoun A. Characterization of different subjects of atrial fibrillation in general practice in France: the ALFA Study. *Circulation*. 1999;99: 3028–3035.
3. Wolf PA, Abbott RD, Kannel WB. Atrial fibrillation as an independent risk factor for stroke: the Framingham Study. *Stroke*. 1991;22:983–988.
4. Connolly SJ, Laupacis A, Gent M, Roberts RS, Cairns JA, Joyner C. Canadian Atrial Fibrillation Anticoagulation (CAFA) Study. *J Am Coll Cardiol*. 1991;18:349–355.
5. Gage BF, Waterman AD, Shannon W, Boechler M, Rich MW, Radford MJ. Validation of clinical classification schemes for predicting stroke: results from the National Registry of Atrial Fibrillation. *JAMA*. 2001; 285:2864–2870.
6. Hohnloser SH, Pajitnev D, Pogue J, Healey JS, Pfeffer MA, Yusuf S, Connolly SJ, for the ACTIVE W Investigators. Incidence of stroke in paroxysmal versus sustained atrial fibrillation in patients taking oral anticoagulation or combined antiplatelet therapy: an ACTIVE W Substudy. *J Am Coll Cardiol*. 2007;50:2156–2161.
7. Fang MC, Go AS, Chang Y, Borowsky L, Pomernacki NK, Singer DE, for the ATRIA Study Group. Comparison of risk stratification schemes to predict thromboembolism in people with nonvalvular atrial fibrillation. *J Am Coll Cardiol*. 2008;51:810–815.
8. Albers GW, Diener HC, Frison L, Grind M, Nevinson M, Partridge S, Halperin JL, Horrow J, Olsson SB, Petersen P, Vahanian A, for the SPORTIF Executive Steering Committee for the SPORTIF V Investigators. Ximelagatran vs warfarin for stroke prevention in patients with nonvalvular atrial fibrillation: a randomized trial. *JAMA*. 2005;293: 690–698.
9. Lewington S, Clarke R, Qizilbash N, Peto R, Collins R, for the Prospective Studies Collaboration. Age-specific relevance of usual blood pressure to vascular mortality: a meta-analysis of individual data for one million adults in 61 prospective studies. *Lancet*. 2002;360:1903–1913.
10. Deroubaix E, Folliguet T, Rücker-Martin C, Dinanian S, Boixel C, Validire P, Daniel P, Capderou A, Hatem SN. Moderate and chronic hemodynamic overload of sheep atria induces reversible cellular electrophysiologic abnormalities and atrial vulnerability. *J Am Coll Cardiol*. 2004;44:1918–1926.
11. Wijffels MC, Kirchhof CJ, Dorland R, Allessie MA. Atrial fibrillation begets atrial fibrillation: a study in awake chronically instrumented goats. *Circulation*. 1995;92:1954–1968.
12. Lang RM, Bierig M, Devereux RB, Flachskampf FA, Foster E, Pellikka PA, Picard MH, Roman MJ, Seward J, Shanewise JS, Solomon SD, Spencer KT, Sutton MS, Stewart WJ, for the Chamber Quantification Writing Group; American Society of Echocardiography's Guidelines and Standards Committee; European Association of Echocardiography. Recommendations for chamber quantification: a report from the American Society of Echocardiography's Guidelines and Standards Committee and the Chamber Quantification Writing Group, developed in conjunction with the European Association of Echocardiography, a branch of the European Society of Cardiology. *J Am Soc Echocardiogr*. 2005;18: 1440–1463.
13. Rodrigues AC, Scannavacca MI, Caldas MA, Hotta VT, Pisani C, Sosa EA, Mathias W Jr. Left atrial function after ablation for paroxysmal atrial fibrillation. *Am J Cardiol*. 2009;103:395–398.
14. Abhayaratna WP, Seward JB, Appleton CP, Douglas PS, Oh JK, Tajik AJ, Tsang TS. Left atrial size: physiologic determinants and clinical applications. *J Am Coll Cardiol*. 2006;47:2357–2363.
15. Manning WJ, Leeman DE, Gotch PJ, Come PC. Pulsed Doppler evaluation of atrial mechanical function after electrical cardioversion of atrial fibrillation. *J Am Coll Cardiol*. 1989;13:617–623.
16. Thomas L, Boyd A, Thomas SP, Schiller NB, Ross DL. Atrial structural remodelling and restoration of atrial contraction after linear ablation for atrial fibrillation. *Eur Heart J*. 2003;24:1942–1951.
17. Nagueh SF, Sun H, Kopelen HA, Middleton KJ, Khoury DS. Hemodynamic determinants of the mitral annulus diastolic velocities by tissue Doppler. *J Am Coll Cardiol*. 2001;37:278–285.
18. Saraiva RM, Yamano T, Matsumura Y, Takasaki K, Toyono M, Agler DA, Greenberg N, Thomas JD, Shiota T. Left atrial function assessed by real-time 3-dimensional echocardiography is related to right ventricular systolic pressure in chronic mitral regurgitation. *Am Heart J*. 2009;158: 309–316.
19. Thomas L, Levett K, Boyd A, Leung DY, Schiller NB, Ross DL. Changes in regional left atrial function with aging: evaluation by Doppler tissue imaging. *Eur J Echocardiogr*. 2003;4:92–100.
20. Khankirawatana B, Khankirawatana S, Peterson B, Mahrous H, Porter TR. Peak atrial systolic mitral annular velocity by Doppler tissue reliably predicts left atrial systolic function. *J Am Soc Echocardiogr*. 2004;17: 353–360.
21. Barbier P, Alioto G, Guazzi MD. Left atrial function and ventricular filling in hypertensive patients with paroxysmal atrial fibrillation. *J Am Coll Cardiol*. 1994;24:165–170.
22. Anwar AM, Geleijnse ML, Soliman OI, Nemes A, ten Cate FJ. Left atrial Frank-Starling law assessed by real-time, three-dimensional echocardiographic left atrial volume changes. *Heart*. 2007;93:1393–1397.
23. Stefanadis C, Dernellis J, Toutouzas P. A clinical appraisal of left atrial function. *Eur Heart J*. 2001;22:22–36.
24. Pickering TG, Hall JE, Appel LJ, Falkner BE, Graves J, Hill MN, Jones DW, Kurtz T, Sheps SG, Roccella EJ, for the Subcommittee of Professional and Public Education of the American Heart Association Council on High Blood Pressure Research. Recommendations for blood pressure measurement in humans and experimental animals: part 1–blood pressure measurement in humans: a statement for professionals from the Subcommittee of Professional and Public Education of the American Heart Association Council on High Blood Pressure Research. *Hypertension*. 2005;45:142–161.
25. Devereux RB, Dahlof B, Levy D, Pfeffer MA. Comparison of enalapril versus nifedipine to decrease left ventricular hypertrophy in systemic hypertension (the PRESERVE Trial). *Am J Cardiol*. 1996;78:61–65.
26. Dokainish H, Zoghbi WA, Lakkis NM, Al-Bakshy F, Dhir M, Quinones MA, Nagueh SF. Optimal noninvasive assessment of left ventricular filling pressures: a comparison of tissue Doppler echocardiography and B-type natriuretic peptide in patients with pulmonary artery catheters. *Circulation*. 2004;109:2432–2439.
27. Pritchett AM, Mahoney DW, Jacobsen SJ, Rodeheffer RJ, Karon BL, Redfield MM. Diastolic dysfunction and left atrial volume: a population-based study. *J Am Coll Cardiol*. 2005;45:87–92.
28. Weber KT, Brilla CG, Janicki JS. Myocardial fibrosis: functional significance and regulatory factors. *Cardiovasc Res*. 1993;27:341–348.
29. Kai H, Kuwahara F, Tokuda K, Imaizumi T. Diastolic dysfunction in hypertensive hearts: roles of perivascular inflammation and reactive myocardial fibrosis. *Hypertens Res*. 2005;28:483–490.
30. Leite-Moreira AF, Correia-Pinto J, Gillebert TC. Afterload induced changes in myocardial relaxation: a mechanism for diastolic dysfunction. *Cardiovasc Res*. 1999;43:344–353.
31. Choisy SC, Arberry LA, Hancox JC, James AF. Increased susceptibility to atrial tachyarrhythmia in spontaneously hypertensive rat hearts. *Hypertension*. 2007;49:498–505.
32. Verdecchia P, Reboldi G, Gattobigio R, Bentivoglio M, Borgioni C, Angeli F, Carluccio E, Sardone MG, Porcellati C. Atrial fibrillation in hypertension: predictors and outcome. *Hypertension*. 2003;41:218–223.
33. Petersen P, Kastrup J, Brinch K, Godtfredsen J, Boysen G. Relation between left atrial dimension and duration of atrial fibrillation. *Am J Cardiol*. 1987;60:382–384.
34. Appleton CP, Jensen JL, Hatle LK, Oh JK. Doppler evaluation of left and right ventricular diastolic function: a technical guide for obtaining optimal flow velocity recordings. *J Am Soc Echocardiogr*. 1997;10: 271–292.
35. De Boeck BW, Cramer MJ, Oh JK, van der Aa RP, Jaarsma W. Spectral pulsed tissue Doppler imaging in diastole: a tool to increase our insight in and assessment of diastolic relaxation of the left ventricle. *Am Heart J*. 2003;146:411–419.
36. Di Salvo G, Caso P, Lo Piccolo R, Fusco A, Martiniello AR, Russo MG, D'Onofrio A, Severino S, Calabró P, Pacileo G, Mininni N, Calabró R. Atrial myocardial deformation properties predict maintenance of sinus rhythm after external cardioversion of recent-onset lone atrial fibrillation: a color Doppler myocardial imaging and transthoracic and transesophageal echocardiographic study. *Circulation*. 2005;112:387–395.

37. Schneider C, Malisius R, Krause K, Lampe F, Bahlmann E, Boczor S, Antz M, Ernst S, Kuck KH. Strain rate imaging for functional quantification of the left atrium: atrial deformation predicts the maintenance of sinus rhythm after catheter ablation of atrial fibrillation. *Eur Heart J.* 2008;29:1397–1409.
38. Eshoo S, Boyd AC, Ross DL, Marwick TH, Thomas L. Strain rate evaluation of phasic atrial function in hypertension. *Heart.* 2009;95: 1184–1191.
39. Thomas L, McKay T, Byth K, Marwick TH. Abnormalities of left atrial function after cardioversion: an atrial strain rate study. *Heart.* 2007;93: 89–95.
40. Kasner M, Westermann D, Steendijk P, Gaub R, Wilkenshoff U, Weitmann K, Hoffmann W, Poller W, Schultheiss HP, Pauschinger M, Tschöpe C. Utility of Doppler echocardiography and tissue Doppler imaging in the estimation of diastolic function in heart failure with normal ejection fraction: a comparative Doppler-conductance catheterization study. *Circulation.* 2007;116:637–647.
41. Quiñones MA, Otto CM, Stoddard M, Waggoner A, Zoghbi WA, for the Doppler Quantification Task Force of the Nomenclature and Standards Committee of the American Society of Echocardiography. Recommendations for quantification of Doppler echocardiography: a report from the Doppler Quantification Task Force of the Nomenclature and Standards Committee of the American Society of Echocardiography. *J Am Soc Echocardiogr.* 2002;15:167–184.
42. Paulus WJ, Tschöpe C, Sanderson JE, Rusconi C, Flachskampf FA, Rademakers FE, Marino P, Smiseth OA, De Keulenaer G, Leite-Moreira AF, Borbély A, Edes I, Handoko ML, Heymans S, Pezzali N, Pieske B, Dickstein K, Fraser AG, Brutsaert DL. How to diagnose diastolic heart failure: a consensus statement on the diagnosis of heart failure with normal left ventricular ejection fraction by the Heart Failure and Echocardiography Associations of the European Society of Cardiology. *Eur Heart J.* 2007;28:2539–2350.
43. Rho RW, Page RL. Asymptomatic atrial fibrillation. *Prog Cardiovasc Dis.* 2005;48:79–87.
44. Hart RG, Pearce LA, Aguilar MI. Meta-analysis: antithrombotic therapy to prevent stroke in patients who have nonvalvular atrial fibrillation. *Ann Intern Med.* 2007;146:857–867.
45. Schnabel RB, Sullivan LM, Levy D, Pencina MJ, Massaro JM, D'Agostino RB Sr, Newton-Cheh C, Yamamoto JF, Magnani JW, Tadros TM, Kannel WB, Wang TJ, Ellinor PT, Wolf PA, Vasan RS, Benjamin EJ. Development of a risk score for atrial fibrillation (Framingham Heart Study): a community-based cohort study. *Lancet.* 2009;373:739–745.

nature
cell biology

AMPK controls the speed of microtubule polymerization and directional cell migration through CLIP-170 phosphorylation

Atsushi Nakano[1,4], Hisakazu Kato[3,4], Takashi Watanabe[5,6], Kyung-Duk Min[1,3], Satoru Yamazaki[1], Yoshihiro Asano[3,4], Osamu Seguchi[1], Shuichiro Higo[3], Yasunori Shintani[3], Hiroshi Asanuma[1], Masanori Asakura[1], Tetsuo Minamino[3], Kozo Kaibuchi[6], Naoki Mochizuki[2], Masafumi Kitakaze[1] and Seiji Takashima[3,4,7]

AMP-activated protein kinase (AMPK) is an energy-sensing Ser/Thr protein kinase originally shown to be regulated by AMP[1]. AMPK is activated by various cellular stresses that inhibit ATP production or stimulate ATP consumption[2]. In addition to its role in metabolism, AMPK has recently been reported to reshape cells by regulating cell polarity and division[3–6]. However, the downstream targets of AMPK that participate in these functions have not been fully identified. Here, we show that phosphorylation of the microtubule plus end protein CLIP-170 by AMPK is required for microtubule dynamics and the regulation of directional cell migration. Both inhibition of AMPK and expression of a non-phosphorylatable CLIP-170 mutant resulted in prolonged and enhanced accumulation of CLIP-170 at microtubule tips, and slower tubulin polymerization. Furthermore, inhibition of AMPK impaired microtubule stabilization and perturbed directional cell migration. All of these phenotypes were rescued by expression of a phosphomimetic CLIP-170 mutant. Our results demonstrate, therefore, that AMPK controls basic cellular functions by regulating microtubule dynamics through CLIP-170 phosphorylation.

Besides the metabolic activity of AMPK, there is growing evidence that AMPK and its upstream kinase liver kinase B1 (LKB1) have pivotal roles in the establishment of cell polarity and cell division[7,8] in *Drosophila melanogaster*[6,9] and *Caenorhabditis elegans*[10]. In mammalian cells, AMPK is associated with tight junction assembly, and regulates epithelial polarity[3,4].

To discover previously unidentified substrates of AMPK, we performed a unique screen using two-step column chromatography combined with an *in vitro* kinase reaction. Using mouse heart homogenates, we purified and identified a cytoplasmic linker protein CLIP-170, which has a relative molecular mass of 170,000 (M_r 170K) and is a substrate of AMPK (Supplementary Information, Fig. S1). CLIP-170 is one of the microtubule plus end proteins originally identified as proteins that bind endocytic vesicles to microtubules[11,12]. CLIP-170 directly binds freshly polymerized distal ends of growing microtubules and rapidly dissociates from the older microtubule lattice[13]. However, a direct link between CLIP-170 and physiological control of cell function has not been fully elucidated. Both recombinant AMPK made by 293T cells and AMPK purified from rat liver efficiently phosphorylated recombinant CLIP-170 (Fig. 1a). Phospho amino acid analysis revealed that AMPK phosphorylates a Ser residue of CLIP-170 (Fig. 1b). A combination of mass spectrometric and multiple mutation analyses of CLIP-170 identified Ser 311 as the only AMPK phosphorylation site. AMPK did not phosphorylate CLIP-115, a close mammalian homologue of CLIP-170, or Ser 737 of CLIP-170, demonstrating an AMPK substrate consensus sequence[14] (Fig. 1c). Recombinant glutathione S-transferase (GST)-fused wild-type CLIP-170 and a Ser 311-to-Ala mutant (S311A) of CLIP-170 were produced in *Escherichia coli*. The wild-type, but not the S311A mutant, was phosphorylated by AMPK and 0.29 mole of phosphate per mole of CLIP-170 was incorporated, indicating that Ser 311 of CLIP-170 is phosphorylated directly by AMPK (Fig. 1d). Next, we generated an antibody against Ser 311-phosphorylated CLIP-170 (p-CLIP-170). The specificity and sensitivity of this antibody were confirmed by the following observations: first the p-CLIP-170 antibody exclusively detected p170 as a single band, even when total cell lysates were assessed; and second, it did not recognize phosphatase-treated p170 (Fig. 1e). Analyses using this antibody also demonstrated the specific phosphorylation of CLIP-170 at Ser 311 by AMPK (Fig. 1f). The amino acid sequence surrounding Ser 311 matches the consensus sequence of a potential AMPK phosphorylation site and is well conserved among various species (Fig. 1g).

[1]Division of Cardiovascular Medicine, National Cardiovascular Center and [2]Department of Structural Analysis, National Cardiovascular Center, Research Institute Suita, Osaka 565-8565, Japan. [3]Department of Cardiovascular Medicine and [4]Department of Molecular Cardiology, Osaka University Graduate School of Medicine Suita, Osaka 565-0871, Japan. [5]Institute for Advanced Research, Nagoya University Graduate School of Medicine and [6]Department of Cell Pharmacology, Nagoya University Graduate School of Medicine, Nagoya, Aichi 466-8550, Japan.
[7]Correspondence should be addressed to S.T. (e-mail: takasima@medone.med.osaka-u.ac.jp)

Received 4 March 2010; accepted 29 April 2010; published online 23 May 2010; DOI: 10.1038/ncb2060

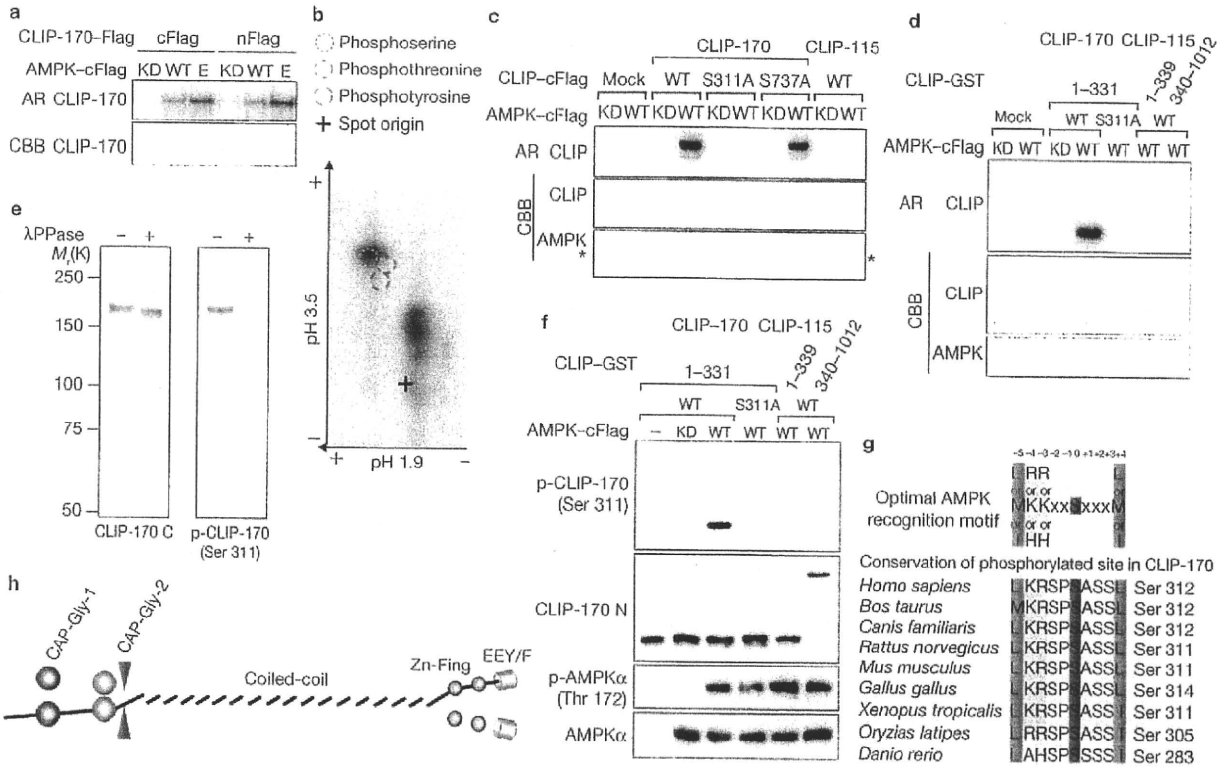

Figure 1 *In vitro* phosphorylation of CLIP-170 Ser311 by AMPK. **(a)** An autoradiographic (AR) image of mammalian recombinant carboxy-terminally (cFlag) or amino-terminally (nFlag) Flag-tagged CLIP-170 incubated with either recombinant kinase dead (KD), wild-type (WT) or endogenous (E) AMPK. **(b)** Phospho-amino acid analysis of CLIP-170 phosphorylated by AMPK. Only a Ser residue was phosphorylated (radioactivity indicated by the red circle). **(c)** An AR of mammalian recombinant cFlag-tagged CLIP-170 (WT, S311A and S737A) and CLIP-115 (WT) incubated with recombinant KD or WT AMPK. AMPK is indicated by an asterisk. **(d)** An AR image of GST fusion proteins representing amino acids 1–331 of CLIP-170 (WT or S311A), or either the N (1–339) or the C (340–1012) terminus of CLIP-115 incubated with KD or WT AMPK. **(e)** Lysate of Vero cells treated with or without phosphatase (λPPase) was subjected to immunoblot analysis with an antibody against the C terminus of CLIP-170 (CLIP-170 C) and a Ser 311 phosphospecific antibody (p-CLIP-170). **(f)** Immunoblot analysis of the GST-fused CLIP constructs described above with KD or WT AMPK. These samples were blotted using a p-CLIP-170 and a non-phosphospecific antibody against the N terminus of CLIP-170 (CLIP-170 N). CLIP-170 N also recognized CLIP-115. **(g)** The optimal AMPK recognition motif. The consensus sequence of AMPK is identical to the sequence around Ser 311 of CLIP-170. This residue is highly conserved among various species. **(h)** Structural model of CLIP-170. Ser 311 is located between the CAP-Gly-2 domain and the coiled-coil region in CLIP-170. Ser 311 is indicated by red arrowheads. CAP-Gly, cytoskeleton-associated protein Gly-rich; Zn-Fing, C-terminal zinc knuckle of CLIP-170; EEY/F, C-terminal amino sequence of CLIP-170; CBB, Coomassie brilliant blue staining. Uncropped images of blots are shown in Supplementary Information, Fig. S5.

Ser 311 is located between a Gly-rich microtubule-binding domain (cytoskeleton-associated protein Gly-rich; CAP-Gly) and a coiled-coil domain (Fig. 1h).

Next, we examined AMPK-induced CLIP-170 phosphorylation in cultured cells. Compound C, an inhibitor of AMPK, reduced the phosphorylation level of CLIP-170 (Fig. 2a), whereas the AMPK activator AICAR (5-aminoimidazole-4-carboxyamide ribonucleoside) did not affect CLIP-170 phosphorylation (Supplementary Information, Fig. S2a). The phosphorylation level of acetyl-CoA carboxylase (ACC), which was used as a control, reflected the conventional responses of cells to both Compound C and AICAR. Although Compound C is an inhibitor of AMPK, it can also inhibit several other kinases[15]. Therefore, we used short interfering RNAs (siRNAs) to specifically deplete AMPK. Depletion of AMPK with siRNAs specific for either the α_1 or the α_2 catalytic subunit also reduced CLIP-170 phosphorylation (Fig. 2b). These data indicate that phosphorylation of CLIP-170 at Ser 311 is regulated endogenously by AMPK. To explore the significance of AMPK-induced CLIP-170 phosphorylation, we first immunocytochemically investigated the localization of phosphorylated CLIP-170 in cultured cells. A non-phospho-specific antibody (CLIP-170 C), as well as a Ser 311 phospho-specific antibody (p-CLIP-170), stained the plus ends of microtubules (Fig. 2c, d). To distinguish between the total CLIP-170 population and phosphorylated CLIP-170, Vero cells stably expressing CLIP-170–EGFP were stained with these antibodies. The pattern observed with the CLIP-170 C antibody (red or yellow) completely matched that of CLIP-170–EGFP (Fig. 2e, green), suggesting that CLIP-170–EGFP mimics the localization of endogenous CLIP-170. By contrast, p-CLIP-170 staining mostly overlapped with CLIP-170–EGFP but was located predominantly on the distal side (red or yellow) of CLIP-170–EGFP (Fig. 2f, green). This result suggests that phosphorylated CLIP-170 attaches to microtubules at the more distal end, compared with non-phosphorylated CLIP-170. A marked change in CLIP-170 localization was observed when these cells were treated with Compound C: CLIP-170–EGFP accumulated significantly farther along the length of the microtubules (Fig. 2g, h, green). CLIP-170 C staining again overlapped with CLIP-170–EGFP (Fig. 2g, red or yellow), whereas p-CLIP-170 staining was markedly reduced and localized as only a tiny

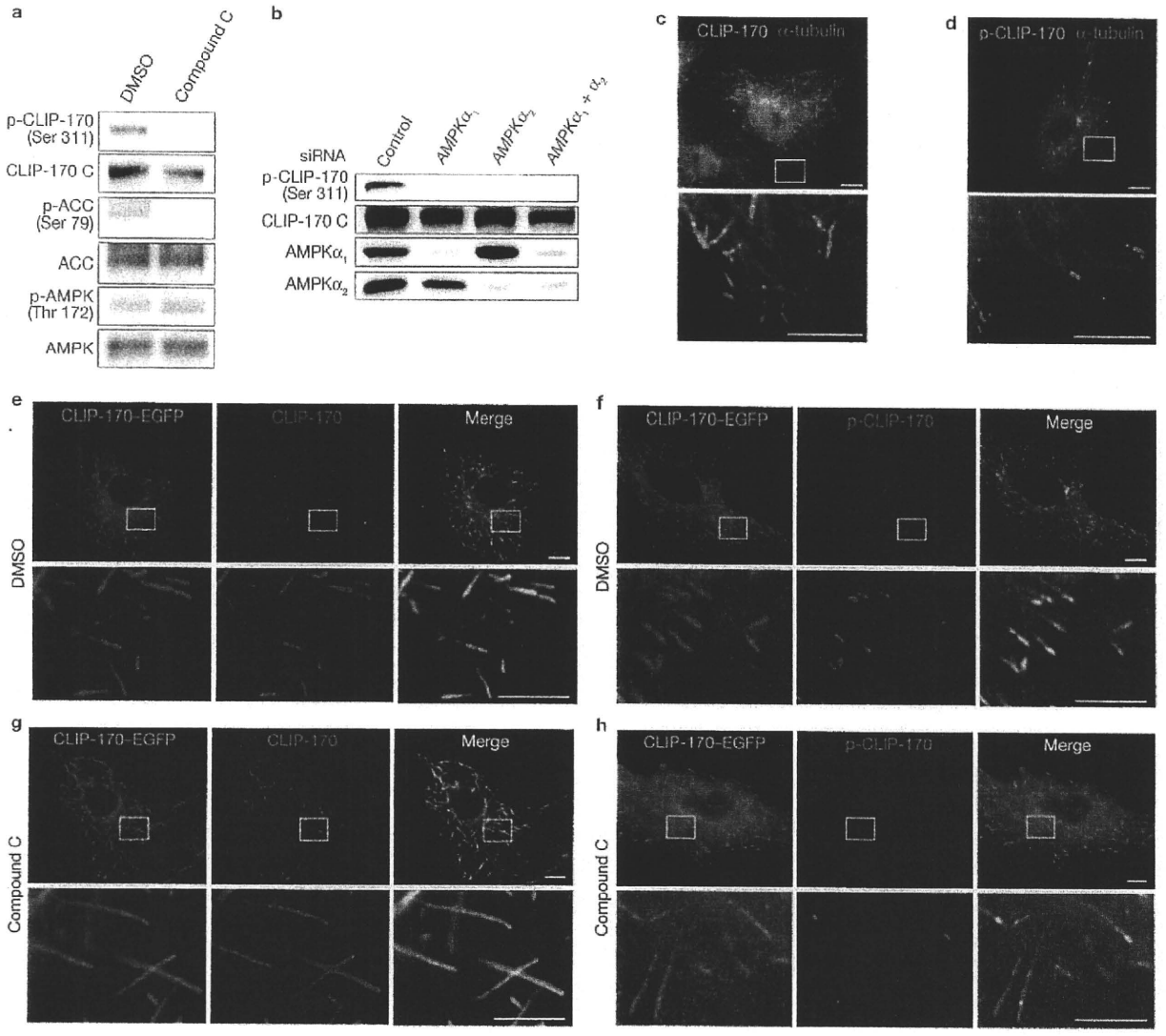

Figure 2 CLIP-170 phosphorylated by AMPK localizes to microtubule tips. (**a**) Immunoblot analysis of the phosphorylation level of CLIP-170, AMPK, and ACC in cells treated with 0.2% DMSO or Compound C (20 μM). CLIP-170 C is a non-phosphospecific antibody that recognizes the C terminus of CLIP-170. (**b**) Immunoblot analysis of the phosphorylation level of CLIP-170 and the expression level of AMPKα_1 and α_2 in cells treated with siRNA targeting *AMPK*α_1, α_2, or both subunits of AMPK. (**c**) Immunostained images of Vero cells stained with anti-α-tubulin and the anti-CLIP-170 C antibodies. (**d**) Immunostained images of Vero cells stained with α-tubulin and p-CLIP-170 antibodies. (**e**, **f**) Immunostained images of Vero cells stably expressing CLIP-170–EGFP (GFP image, left) and treated with DMSO as a control. These cells were stained with a CLIP-170 C antibody (**e**, centre) or a p-CLIP-170 antibody (**f**, centre). (**g**, **h**) Immunostained images of Vero cells stably expressing CLIP-170–EGFP (GFP image, left) and treated with Compound C. These cells were stained with a CLIP-170 C antibody (**g**, centre) or a p-CLIP-170 antibody (**h**, centre). The merged images of each panel are shown on the right. The white boxed regions in the panels are enlarged below each panel. Scale bars, 10 μm (**c**–**h**, upper rows) and 5 μm (**c**–**h**, bottom rows). Uncropped images of blots are shown in Supplementary Information, Fig. S5.

spot within the CLIP-170–EGFP-positive region (Fig. 2h, red or yellow). Most of the CLIP-170 on microtubules, therefore, was non-phosphorylated, and a small amount of phosphorylated CLIP-170 accumulated at the distal ends. To examine the precise distribution of CLIP-170 on the microtubules under AMPK-inhibited conditions, linescan analysis along the microtubules was performed using double immunocytochemistry with CLIP-170 C and tubulin antibodies. We separately measured total CLIP-170 associated with microtubule plus ends, and CLIP-170 associated with the outermost microtubule tips (within a 0.129-μm square box at the very end of the microtubules). When compared with the DMSO control Compound C treatment increased the association of CLIP-170 with microtubules both in the whole tip (6-fold) and at the outer tip (1.7-fold) (Supplementary Information, Fig. S2b–d). Depletion of both AMPKα_1 and α_2 by siRNA also resulted in accumulation of CLIP-170 on microtubule plus ends, similarly to inhibition by Compound C (Supplementary Information, Fig. S2e, f). This characteristic change of CLIP-170 localization prompted us to examine the role of AMPK in the regulation of microtubule dynamics.

To study how AMPK regulates microtubule dynamics, we examined the behaviour of CLIP-170 in living cells. First, we tested whether phosphorylation levels of CLIP-170 affected polymerization of microtubules.

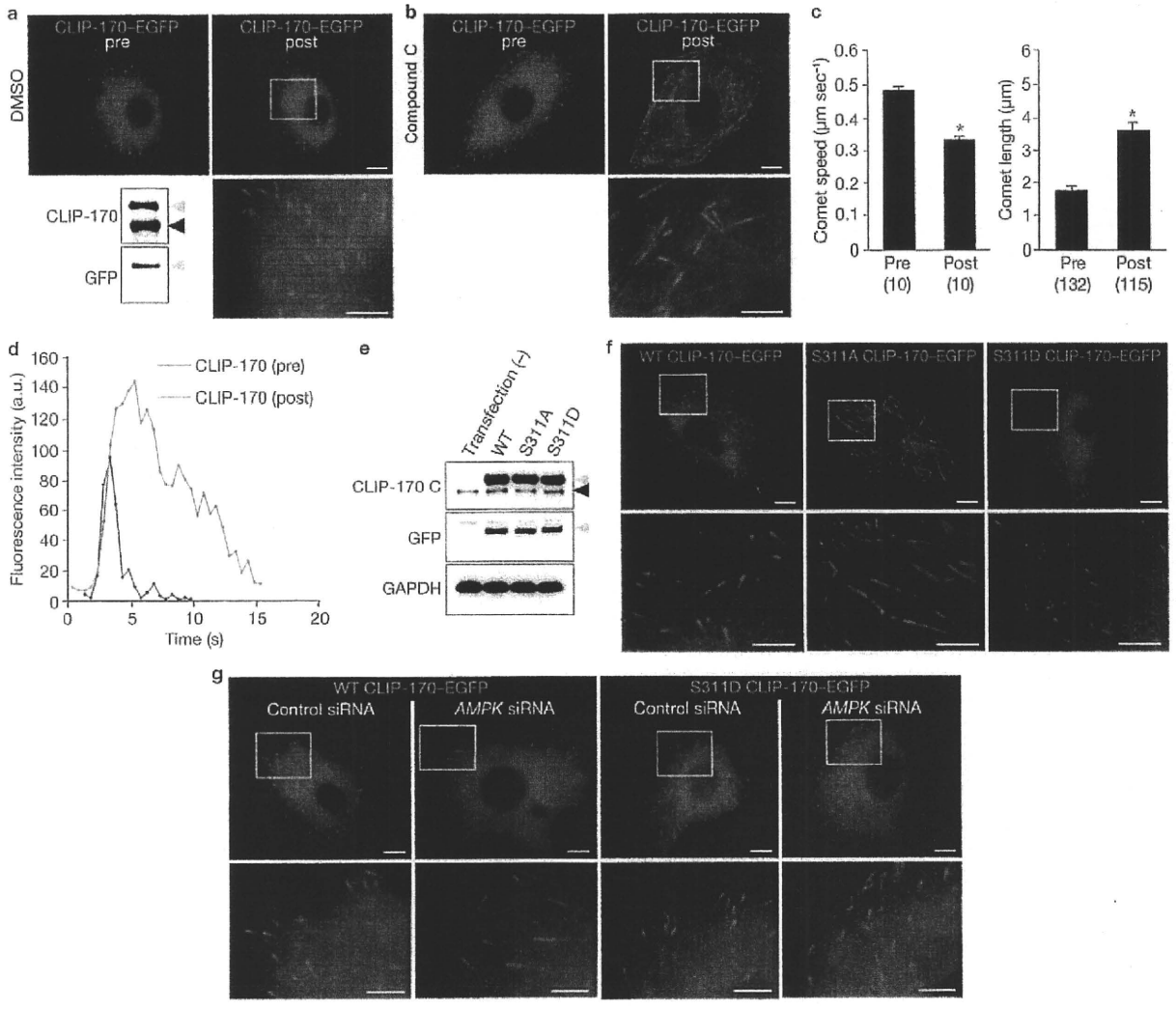

Figure 3 AMPK-phosphorylated CLIP-170 regulates microtubule dynamics. (**a**, **b**) GFP images of Vero cells stably expressing CLIP-170–EGFP before (pre) and 10 min after (post) treatment with 0.2% DMSO control (**a**) or Compound C (20 μM, **b**). The immunoblot on the left shows exogenous CLIP-170–EGFP (grey arrowheads) and endogenous CLIP-170 (black arrowhead). (**c**) Bar graphs showing the speed (left panel) and length (right panel) of a single comet before (pre) and 10 min after (post) Compound C treatment in the same cell. Values are means ± s.e.m.; *n* shown in parentheses; $^*P < 0.01$, compared with pre. (**d**) Fluorescence intensity plots of CLIP-170–EGFP of the same cell before (pre, blue) and 10 min after (post, red) Compound C treatment. (**e**) Expression levels of wild-type (WT), S311A and S311D CLIP-170–EGFP in transiently transfected Vero cells were comparable, as determined by immunoblotting using the antibodies indicated on the left. The grey and black arrowheads indicate GFP-tagged exogenous CLIP-170 and endogenous CLIP-170, respectively. (**f**) GFP images of cells transiently expressing WT (left), S311A (centre) and S311D (right) CLIP-170–EGFP. (**g**) GFP images of the cells transiently expressing WT and S311D CLIP-170–EGFP treated with control siRNA or siRNA targeting both *AMPK*α_1 and α_2. White boxed regions in the panels are enlarged below each panel. Scale bars, 10 μm (**a**, **b**, **f**, **g**, upper panels) and 5 μm (**a**, **b**, **f**, **g**, enlarged images). Uncropped images of blots are shown in Supplementary Information, Fig. S5.

By live-cell imaging, we observed that stably expressed CLIP-170–EGFP accumulated at the distal ends of microtubules and seemed to move like a comet from the centrosome to the cell periphery (as shown in sequential images converted to video, Supplementary Information, Movie 1). The speed of the CLIP-170 comets coincided with that of microtubule polymerization[16,17]. Consistent with our results in fixed cells (Fig. 2), 10-min inhibition of AMPK by Compound C in living cells also resulted in elongated CLIP-170 comets, compared with control DMSO-treated cells (Fig. 3a–c). Moreover, the speed of the comets was reduced by Compound C (Fig. 3c; Supplementary Information, Movie 2). To analyse the CLIP-170 behaviour more precisely, we measured the fluorescence intensity values along the CLIP-170–EGFP tracks over time in the same living cells before and 10 min after Compound C treatment. This fluorescence intensity analysis of CLIP-170–EGFP demonstrated that Compound C markedly increased the peak fluorescence intensity and slowed the dissociation of CLIP-170 from the older part of the microtubules (Fig. 3d). Using the same cell line stably expressing CLIP-170–EGFP, depletion of AMPK by siRNA also reduced the speed of the comets and increased the length of CLIP-170 comets (Supplementary Information, Fig. S2g–i, Movie 3). To elucidate the specific role of CLIP-170 Ser 311 phosphorylation by AMPK, we compared the phenotypes of cells transiently transfected with wild-type and two Ser 311 mutants of CLIP-170. S311A CLIP-170–EGFP

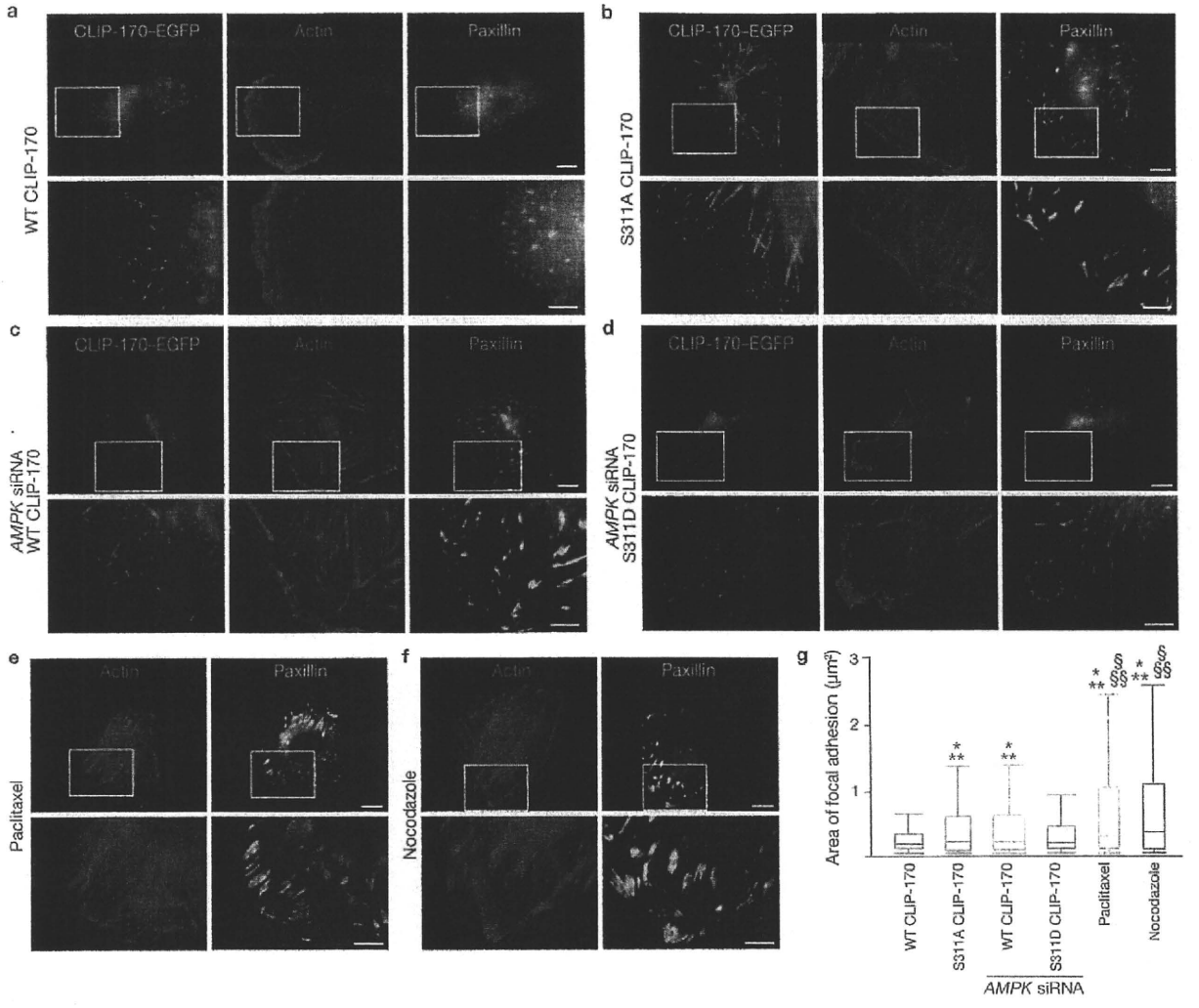

Figure 4 Loss of CLIP-170 phosphorylation increases the size of focal adhesions. (**a**, **b**) Immunostained images of Vero cells transiently expressing wild-type (WT; **a**) and S311A (**b**) CLIP-170–EGFP (GFP image, left). These cells were stained with fluorescein-conjugated phalloidin (centre) and a paxillin antibody (right) to visualize actin microfilaments and focal adhesions, respectively. (**c**, **d**) Immunostained images of Vero cells transiently expressing WT (**c**) and S311D (**d**) CLIP-170–EGFP (GFP image, left) treated with siRNA targeting both *AMPK*α_1 and α_2. These cells were stained with fluorescein-conjugated phalloidin (centre) and a paxillin antibody (right). (**e**, **f**) Immunostained images of Vero cells treated with 5 μM paclitaxel (**e**) or 10 μM nocodazole (**f**). These cells were stained with fluorescein-conjugated phalloidin (left) and a paxillin antibody (right). The white boxed regions in the panels are enlarged below each panel. Scale bars, 10 μm (**a**–**f**, upper row) and 5 μm (**a**–**f**, bottom row). (**g**) Box and whisker plots of the area stained with a paxillin antibody showing the 25th percentile (bottom line of each box), median (middle line of each box), 75th percentile (top line of each box), and the 5th and 95th percentiles (each whisker); $n = 10$ for each group; $^{*}P<0.01$, compared with WT CLIP-170; $^{**}P<0.01$, compared with S311D CLIP-170 treated with *AMPK* siRNA; $^{\S}P<0.01$, compared with S311A CLIP-170; $^{\S\S}P<0.01$, compared with WT CLIP-170 treated with *AMPK* siRNA.

is a non-phosphorylatable mutant, and a Ser 311-to-Asp mutant (S311D CLIP-170–EGFP) is a phosphomimetic mutant. These EGFP fusion proteins were equally expressed in Vero cells (Fig. 3e). S311A CLIP-170–EGFP accumulated as comets with longer tails and moved more slowly than wild-type CLIP-170–EGFP (Fig. 3f centre; Supplementary Information, Table S1, Movie 4). By contrast, S311D CLIP-170–EGFP had the same comet length and moved with the same speed as wild-type CLIP-170–EGFP (Fig. 3f, right; Supplementary Information, Table S1, Movie 5). These findings are consistent with the observation that most of the endogenous CLIP-170 was phosphorylated by AMPK. Furthermore, S311D CLIP-170–EGFP rescued the phenotypes caused by siRNA depletion of AMPK (Fig. 3g; Supplementary Information, Table S1, Movie 6). Also, in the cells treated with Compound C, transfection of S311D CLIP-170–EGFP restored comet speed and length. Quantitative data of comet speed and length in various conditions are summarized in Supplementary Information, Table S1.

CLIP-170 binds only to the growing phase of microtubules. To further examine microtubule dynamics during the shortening phase, Vero cells stably expressing α-tubulin–EGFP were observed before and 10 min after Compound C treatment. Compound C markedly decreased the microtubule shortening distance (Supplementary Information, Fig. S2j, Movie 7). This change in microtubule behaviour may stabilize microtubules. We then observed microtubule stability by staining them with an antibody against detyrosinated tubulin (Glu tubulin,

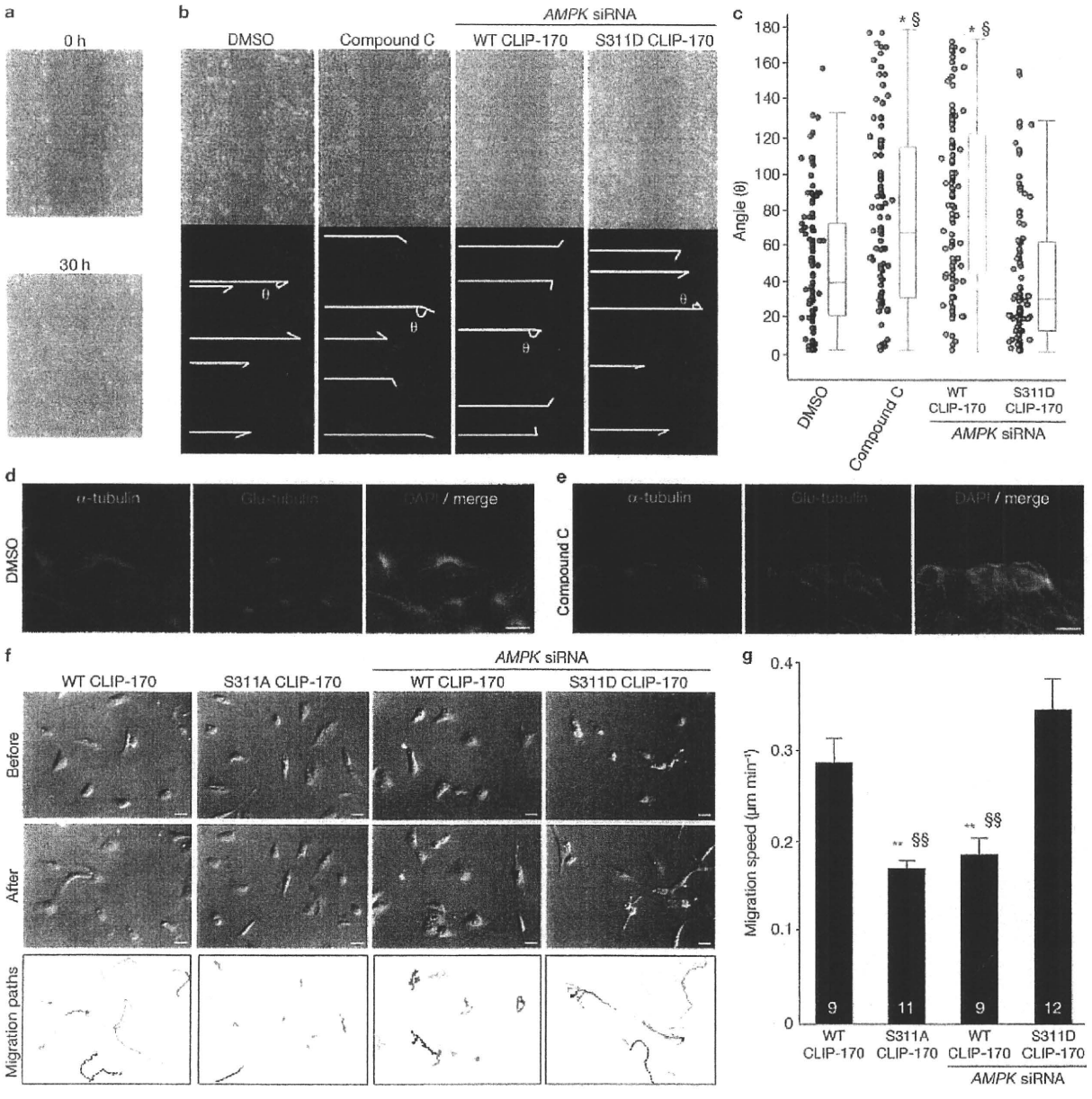

Figure 5 Phosphorylation of CLIP-170 at Ser 311 is essential for cell polarity and directional cell migration. (**a**) Phase contrast microscopy images of Vero cells before (upper panel) and 30 h after (lower panel) scratch. (**b**) Phase contrast microscopy images (upper panels) and immunostained images of Vero cells stained with a γ-tubulin antibody (lower panels) after being subjected to a scratch assay. Images were captured 12 h after incubation. The cells were treated by either repeated administration of DMSO control or Compound C, or transiently transfected with wild-type (WT) or S311D CLIP-170 and siRNA targeting both $AMPK\alpha_1$ and α_2. To assess cell polarity, the angles (θ) between the lines of γ-tubulin and the scratched line at the centre of each nucleus were measured as a marker for MTOC reorientation (lower panels). (**c**) Box and whisker plots of angles (θ) with actual data points shown on the left; n=100 per group; $^{*}P$ <0.01, compared with DMSO; $^{\S}P$ <0.01, compared with S311D CLIP-170 treated with *AMPK* siRNA. (**d**, **e**) Images of Vero cells immunostained with an α-tubulin (left, green) and a detyrosinated (Glu) tubulin antibody (centre, red) after being subjected to a scratch assay following repeated treatment with control DMSO (**d**) or Compound C (**e**) for 6 h. DAPI stained nucleus (blue). The merged images of each panel are shown on the right. Scale bars, 20 μm. (**f**) Time lapse images acquired by differential interference contrast of cells transiently expressing WT, S311A, and WT or S311D CLIP-170 treated with siRNA targeting both $AMPK\alpha_1$ and α_2. Images acquired before (upper line of each panel) and after 12 h (middle line of each panel) are shown. The bottom row of each panel shows the individual paths of migrating cells over 12 h. Scale bars, 30 μm. (**g**) Bar graphs showing the migration speed of the cells from (f); Numbers in the bars indicate n. Values represent means ± s.e.m; $^{**}P$ <0.01, compared with WT CLIP-170. $^{\S\S}P$ <0.01, compared with S311D CLIP-170 treated with *AMPK* siRNA.

named for the newly exposed C-terminal glutamate residue). The amount of stable microtubules was greater in cells transiently expressing S311A CLIP-170–EGFP (Supplementary Information, Fig. S3b) than in cells transiently expressing wild-type CLIP-170 (Supplementary Information, Fig. S3a). Cell depleted of AMPK by siRNA (Supplementary Information, Fig. S3g), or treated with Compound C (Supplementary

Information, Fig. S3d) also showed the same phenotype as cells expressing S311A CLIP-170. These phenotypes were rescued by S311D CLIP-170 (Supplementary Information, Fig. S3f, i). Collectively, these data suggest that phosphorylation of CLIP-170 at Ser 311 by AMPK is necessary for proper CLIP-170 dissociation from microtubules, and that this modification of CLIP-170 is essential for efficient polymerization and depolymerization of microtubules. Dynamic modulation of microtubule polymerization and stability by AMPK-phosphorylated CLIP-170 might represent a previously unknown mechanism through which AMPK establishes cell polarity. Therefore, we further examined the role of CLIP-170 phosphorylation by AMPK during cell polarization and subsequent cell migration.

During cell migration, microtubules target focal adhesions and regulate cell–extracellular matrix (ECM) adhesion[18–20]. Thus, we first examined whether phosphorylation of CLIP-170 at Ser 311 affects the size of focal adhesions. Isolated Vero cells transiently expressing wild-type CLIP-170–EGFP formed an actin meshwork in protruding lamellipodium. Furthermore, staining focal adhesions with a paxillin antibody revealed small, scattered spots located predominantly at the protruding lamellipodium (Fig. 4a). By contrast, expression of S311A CLIP-170–EGFP caused loss of lamellipodium formation and adhesion maturation, which resulted in significantly enlarged spots (Fig. 4b). Similar phenotypes were observed when AMPK was depleted by siRNA (Fig. 4c) or inhibited by Compound C (Supplementary Information, Fig. S4b). These AMPK depletion phenotypes were almost completely rescued by the expression of S311D CLIP-170–EGFP (Fig. 4d, g; Supplementary Information, Fig. S4d). Treatment with paclitaxel and nocodazole (Fig. 4e, f), both of which disturb microtubule dynamics, resulted in similar phenotypes of abnormal size of focal adhesion as cells expressing S311A CLIP-170–EGFP and cells depleted of AMPK. These data indicate that AMPK-dependent phosphorylation of CLIP-170 regulates the size of focal adhesions by regulating microtubule dynamics. The fact that inhibiting AMPK-induced phosphorylation of CLIP-170 altered the size of focal adhesions and lamellipodium formation suggests an important role of the AMPK–CLIP-170 signalling axis in cell polarity and migration. We examined the effect of AMPK inhibition on cell polarity using the scratch assay. The leading cells started to polarize and migrated towards a scratched line, closing the gap in about 30 h (Fig. 5a). However, repeated treatment with Compound C and depletion of AMPK by siRNA both inhibited closure of the gap and interfered with microtubule-organizing centre (MTOC) reorientation in leading cells. Expression of S311D CLIP-170 rescued AMPK depletion (Fig. 5b, c; Supplementary Information, Fig S4g, h). The first two layers of the leading cells showed that the stabilized microtubules stained with a detyrosinated (anti-Glu) tubulin antibody were clearly polarized towards the leading edge (Fig. 5d). By contrast, AMPK inhibition by Compound C increased the amount of stable microtubules, which lost their orientation towards the leading edge (Fig. 5e). Finally, we tested the effect of CLIP-170 phosphorylation on free cell migration. Wild-type CLIP-170-expressing cells migrated with active lamellipodium formation. By contrast, S311A CLIP-170-expressing cells and wild-type CLIP-170-expressing cells treated with *AMPK* siRNA showed diminished migration and fewer membrane extensions (Fig. 5f). Again, expression of S311D CLIP-170 rescued the effect of siRNA *AMPK* knockdown of (Fig. 5g; Supplementary Information, Movie 8). These data suggest that AMPK-induced phosphorylation of CLIP-170 is required to establish front–rear polarity and proper cell migration, presumably through the regulation of microtubule tip dynamics.

We have shown here that CLIP-170 is a strong candidate AMPK substrate that regulates cell polarity through alteration of its dynamics on the plus ends of microtubules. Recently, abnormal mitotic phenotypes were observed for both *AMPK*- and *LKB1*-null *Drosophila*. They demonstrated that AMPK phosphorylates myosin regulatory light chain (MRLC) directly, and a phosphomimetic MRLC transgene rescued the polarity phenotypes induced by loss of the AMPK pathway[6]. However, the transgene did not rescue all phenotypes, suggesting that AMPK signalling is mediated by additional downstream targets.

The dynamics of CLIP-170 on microtubules were recently and precisely investigated both *in vitro* and *in vivo*[15,17]. In these reports, CLIP-170 turnover on microtubules was rapid, and the diffusion of CLIP-170 was rate-limiting for its binding to microtubule plus ends. They also showed that the ends of growing microtubules contain a surplus of sites to which CLIP-170 can bind, and the older lattice has a lower affinity for CLIP-170 than the newer, growing ends of the microtubules. These changes in the affinity of plus end proteins for microtubules may be essential for their effects on microtubule dynamics.

We could not demonstrate an altered affinity of phosphorylated CLIP-170 for the microtubule plus end *in vitro* because of the difficulty associated with reconstituting the plus end as *in vivo*. However, we speculate, for the following reasons, that non-phosphorylated CLIP-170 increased its affinity to microtubules. First, linescan analysis showed that depletion of AMPK activity increased the association not only of total CLIP-170 with the microtubule but also of CLIP-170 at the outer tip. Second, the fluorescence intensity analysis measured in living cells indicated that non-phosphorylated CLIP-170 increased the peak fluorescence intensity and slowed its dissociation from the plus end of microtubules. Third, phosphorylated CLIP-170 localized within the more distal portion of the total CLIP-170 population. These results support the hypothesis that the phosphorylation status of CLIP-170 at Ser 311 determines its affinity for microtubules. Because CLIP-170 turnover on microtubules is rapid, phosphorylation may be a suitable modification to regulate its affinity for microtubules. We conclude that phosphorylation of CLIP-170 alters its affinity for microtubule plus ends and that this phenomenon might contribute to the rapid turnover of CLIP-170, which is necessary for efficient microtubule polymerization.

The observation that the phosphorylation status of CLIP-170 regulates the growth rate of microtubules has not been reported. The precise mechanisms remain unclear; however we speculate that Ser 311 phosphorylation is necessary to reduce the affinity of CLIP-170 for the microtubule lattice and promote the efficient turnover of CLIP-170 at the plus end, similarly to a microtubule polymerase.

Another intriguing phenotype of AMPK depletion is the marked enhancement of microtubule stabilization in migrating cells. Moreover, AMPK depletion impaired the polarized stabilization of microtubules towards the leading edge. AMPK depletion not only reduced the speed of polymerization but also decreased the shortening distance of microtubules. Because both phenomena prolong the lifetime of microtubules, these two changes might cause the ubiquitous enhancement of microtubule stabilization.

Expression of the non-phosphorylatable CLIP-170 S311A mutant and depletion of AMPK disrupted front–rear polarity and reduced cell migration. The precise mechanisms of this phenotype are unclear, but decreased

microtubule polymerization and unpolarized microtubule stabilization might affect the function of microtubules, which are required to establish cell polarity. We have shown that inhibiting CLIP-170 phosphorylation resulted in significant enlargement of focal adhesions, as detected with a paxillin antibody. Enlarged focal adhesions are similar to the phenotype observed in cells treated with paclitaxel or nocodazole, both of which disrupt microtubule dynamics. Microtubules bind to paxillin and help the cell adhesion system to destabilize focal adhesions and promote cell motility[21,22]. These functions suggest that microtubules play a key part in cell polarity and migration through interactions with focal adhesion molecules. Taken together, the results suggest that AMPK promotes the appropriate formation of focal adhesions, the subsequent establishment of cell polarity, and directional cell migration through efficient polymerization of microtubules, by phosphorylating CLIP-170 at Ser 311.

Under normal cell culture conditions, neither enhanced activation of AMPK by AICAR nor S311D CLIP-170–EGFP altered microtubule dynamics, indicating a high basal phosphorylation of CLIP-170. This might be caused by a high affinity of AMPK for CLIP-170, or colocalization of AMPK and CLIP-170.

The results of our broad substrate screening method suggest that CLIP-170 is one of the most important substrates of AMPK in various organs. We believe that observing microtubule dynamics is necessary to evaluate multiple functions of AMPK. Also, similarly to paclitaxel or nocodazole treatment, strong inhibition of microtubule dynamics by the CLIP-170 S311A mutant may have clinical implications. The interaction between AMPK and CLIP-170 might be a therapeutic target for treatment of conditions such as cancer, tumour angiogenesis and neointimal hyperplasia. □

METHODS

Methods and any associated references are available in the online version of the paper at http://www.nature.com/naturecellbiology/

Note: Supplementary Information is available on the Nature Cell Biology website.

ACKNOWLEDGEMENTS

We thank M. Amano and S. Fukuhara for helpful discussions, and M. Koyama (Olympus Corporation) for technical advice regarding microscopy. This research was supported by: a Grants-in-Aid from the Ministry of Health, Labour and Welfare of Japan; Grants-in-Aid from the Ministry of Education, Culture, Sports, Science and Technology of Japan; grants from the Japan Heart Foundation; grants from the Japan Cardiovascular Research Foundation; a grant from the Japan Society for the Promotion of Science; a grant from the Mochida Memorial Foundation for Medical and Pharmaceutical Research; and a Grant-in-Aid from the Japan Medical Association.

AUTHOR CONTRIBUTIONS

A.N. designed and conducted the study, performed most of the experiments, and wrote the manuscript; S.T. designed and conducted the study, performed the biochemical experiments and wrote the manuscript; H.K. carried out immunoblot analysis; K.M. independently counted the number of cells; S.Y. helped to generate the plasmids; Y.A., O.S., S.H., Y.S., H.A., M.A. and T.M. discussed the results and reviewed the manuscript; T.W. and K.K. generated and provided antibodies and Vero cells and reviewed the manuscript; N.M. conducted and supported the biological experiments and wrote the manuscript; M.K. supervised all work.

COMPETING INTERESTS

The authors declare no competing financial interests.

Published online at http://www.nature.com/naturecellbiology/
Reprints and permissions information is available online at http://npg.nature.com/reprintsandpermissions/

1. Yeh, L. A., Lee, K. H. & Kim, K. H. Regulation of rat liver acetyl-CoA carboxylase. Regulation of phosphorylation and inactivation of acetyl-CoA carboxylase by the adenylate energy charge. *J. Biol. Chem.* **255**, 2308–2314 (1980).
2. Hardie, D. G. AMP-activated/SNF1 protein kinases: conserved guardians of cellular energy. *Nature Rev. Mol. Cell Biol.* **8**, 774–785 (2007).
3. Zhang, L., Li, J., Young, L. H. & Caplan, M. J. AMP-activated protein kinase regulates the assembly of epithelial tight junctions. *Proc. Natl Acad. Sci. USA* **103**, 17272–17277 (2006).
4. Zheng, B. & Cantley, L. C. Regulation of epithelial tight junction assembly and disassembly by AMP-activated protein kinase. *Proc. Natl Acad. Sci. USA* **104**, 819–822 (2007).
5. Mirouse, V., Swick, L. L., Kazgan, N., St. Johnston, D. & Brenman, J. E. LKB1 and AMPK maintain epithelial cell polarity under energetic stress. *J. Cell Biol.* **177**, 387–392 (2007).
6. Lee, J. H. *et al.* Energy-dependent regulation of cell structure by AMP-activated protein kinase. *Nature* **447**, 1017–1020 (2007).
7. Williams, T. & Brenman, J. E. LKB1 and AMPK in cell polarity and division. *Trends Cell Biol.* **18**, 193–198 (2008).
8. Jansen, M., Ten Klooster, J. P., Offerhaus, G. J. & Clevers, H. LKB1 and AMPK family signaling: the intimate link between cell polarity and energy metabolism. *Physiol. Rev.* **89**, 777–798 (2009).
9. Martin, S. G. & St. Johnston, D. A role for *Drosophila* LKB1 in anterior–posterior axis formation and epithelial polarity. *Nature* **421**, 379–384 (2003).
10. Watts, J. L., Morton, D. G., Bestman, J. & Kemphues, K. J. The *C. elegans par-4* gene encodes a putative serine-threonine kinase required for establishing embryonic asymmetry. *Development* **127**, 1467–1475 (2000).
11. Rickard, J. E. & Kreis, T. E. Identification of a novel nucleotide-sensitive microtubule-binding protein in HeLa cells. *J. Cell Biol.* **110**, 1623–1633 (1990).
12. Pierre, P., Scheel, J., Rickard, J. E. & Kreis, T. E. CLIP-170 links endocytic vesicles to microtubules. *Cell* **70**, 887–900 (1992).
13. Dragestein, K. A. *et al.* Dynamic behavior of GFP-CLIP-170 reveals fast protein turnover on microtubule plus ends. *J. Cell Biol.* **180**, 729–737 (2008).
14. Hardie, D. G., Carling, D. & Carlson, M. The AMP-activated/SNF1 protein kinase subfamily: metabolic sensors of the eukaryotic cell? *Annu. Rev. Biochem.* **67**, 821–855 (1998).
15. Bain, J. *et al.* The selectivity of protein kinase inhibitors: a further update. *Biochem. J.* **408**, 297–315 (2007).
16. Perez, F., Diamantopoulos, G. S., Stalder, R. & Kreis, T. E. CLIP-170 highlights growing microtubule ends *in vivo*. *Cell* **96**, 517–527 (1999).
17. Bieling, P. *et al.* CLIP-170 tracks growing microtubule ends by dynamically recognizing composite EB1/tubulin-binding sites. *J. Cell Biol.* **183**, 1223–1233 (2008).
18. Wu, X., Kodama, A. & Fuchs, E. ACF7 regulates cytoskeletal-focal adhesion dynamics and migration and has ATPase activity. *Cell* **135**, 137–148 (2008).
19. Rodriguez, O. C. *et al.* Conserved microtubule–actin interactions in cell movement and morphogenesis. *Nat. Cell Biol.* **5**, 599–609 (2003).
20. Small, J. V., Geiger, B., Kaverina, I. & Bershadsky, A. How do microtubules guide migrating cells? *Nature Rev. Mol. Cell Biol.* **3**, 957–964 (2002).
21. Turner, C. E. Paxillin and focal adhesion signalling. *Nat. Cell Biol.* **2**, E231–E236 (2000).
22. Broussard, J. A., Webb, D. J. & Kaverina, I. Asymmetric focal adhesion disassembly in motile cells. *Curr. Opin. Cell Biol.* **20**, 85–90 (2008).

molecular signaling mechanisms involved in the unfolded protein response have not been fully identified in diseased hearts. Recently, we have demonstrated that expression of ER chaperones was increased and CHOP was induced in experimental heart failure.[9] CHOP has been identified as an ER-initiated proapoptotic signal that plays an important role in the pathophysiology of diabetes mellitus and neurodegenerative diseases.[3,10,11] Furthermore, CHOP can also directly regulate death effectors such as Bcl2, which is one of key determinants of cell death or survival.[12] Although the apoptosis of cardiomyocytes may contribute to the development of heart failure,[13–16] the role of ER-initiated apoptosis in the pathophysiology of heart failure remains unclear. In the present study, we investigated ER stress signaling in human hearts. We also performed in vivo studies to clarify the pathophysiological role of CHOP in the development of cardiac hypertrophy and failure and examined the potential downstream signaling of CHOP in pressure-overloaded hearts of mice.

Methods

Materials

Antibodies for CHOP, Bax, Bcl2, ATF4, ATP5α, and actin were obtained from Santa Cruz Biotechnology (Santa Cruz, Calif); antibodies for phospho-SAPK/JNK, SAPK/JNK, phospho-eIF2α, eIF2α, and cleaved caspase-3 were obtained from Cell Signaling Technology, Inc (Danvers, Mass). Isoproterenol and the antibody for caspase-12 were obtained from Sigma Chemical Corp (St. Louis, Mo). Antibodies for BiP and GAPDH were purchased from Assay Designs, Inc (Ann Arbor, Mich) and Millipore Corp (Billerica, Mass), respectively.

Human Heart Samples

Human heart samples were studied according to the protocol approved by the Institutional Review boards of the National Cardiovascular Center (No. 14 to 18) and Hayama Heart Center. For quantitative real-time reverse-transcription polymerase chain reaction (PCR), we used surgical samples of myocardium removed from 12 patients with dilated cardiomyopathy and 3 patients with ischemic cardiomyopathy who underwent left ventriculoplasty at the Hayama Heart Center. Six control heart samples for quantitative real-time PCR were obtained from BD Biosciences (San Jose, Calif). Tissues were frozen at −80°C until use for extraction of RNA.

Animal Preparation

Mice lacking the *CHOP* gene were generated on a C57BL/6 background as described previously.[17] Experiments were performed with CHOP-deficient mice and littermate control mice. All procedures were done in accordance with the guiding principles of Osaka University School of Medicine with regard to animal care and the "Position of the American Heart Association on Research Animal Use."

Transverse Aortic Constriction

Pressure overload of the heart was induced in 10-week-old male mice (20 to 25 g) by transverse aortic constriction (TAC) as described previously.[18,19]

Immunohistological Analysis

Immunohistological analysis was performed as described previously.[18,19]

Echocardiography

Cardiac function was assessed by Doppler echocardiography with a 15-MHz transducer (Philips, SONOS5500, Eindhoven, the Netherlands).[18,19]

Preparation of Neonatal Rat Cardiomyocytes

Primary cardiomyocyte cultures were prepared from neonatal rat hearts.[20] We used short interfering RNA (siRNA) (cocktail containing equal amounts of the 3 types of siRNA—5′-CGAAGAGGAAGAAUCAAA-3′, 5′-GGAAACAGCGACUGAAGGA-3′, and 5′-GGGACUGAGGGUAGACCAA-3′)—to knock down *CHOP* messenger RNA (mRNA) as described previously.[20] Cardiomyocytes were stained with rhodamine-phalloidin (Invitrogen Corp, Carlsbad, Calif).

Measurement of Contractility With Isolated Adult Mice Cardiomyocytes

Adult cardiomyocytes were isolated from 8-week-old wild-type (WT) or CHOP knockout mice and were stored in Hanks buffer (Invitrogen Corp) containing 1.2 mmol/L $CaCl_2$. Field stimulation at 1-Hz pacing rate was done with 5-ms square pulses of constant voltage at 20% above threshold.[21] Changes in cell length during contracting and relaxing were recorded with an inverted microscopy (Olympus IX81, Olympus Corp, Tokyo, Japan) and analyzed with Metamorph software (Molecular Devices Corp, Tokyo, Japan). Cell shortening was calculated as follows: (relaxing length−contracting length)/relaxing length.

Quantitative Real-Time PCR

Quantitative real-time PCR of human heart tissue was performed according to the Omniscript Reverse Transcription Handbook (Qiagen Inc, Valencia, Calif). The primers and probes used for quantification of *BiP*, *ATF4*, *CHOP*, and *GAPDH* were all designed according to the manufacturer's protocol (Applied Biosystems, Foster City, Calif; https://www.appliedbiosystems.com/catalog/). Quantitative real-time PCR for the detection of *GADD34* was performed with QuantiTect SYBR Green Kit (Qiagen, Inc) with the following primers: *GADD34*: forward, ATCTCCTGAACAGAGTCAAGCAGCCCAGAG; reverse, TAGCCACCACCTCCCCAAGCCTCTTATCAG; *GAPDH*: forward, CATCAACGACCCCTTCATTGACCTCAACTA; reverse, TCCACGATGCCAAAGTTGTCATGGATGACC. Quantitative real-time PCR was performed with an ABI PRISM 7000 Sequence Detection System (Applied Biosystems) by the relative standard curve method. The reaction was performed at 50°C for 2 minutes and 95°C for 10 minutes, followed by 40 cycles at 95°C for 15 seconds and 60°C for 1 minute. The amount of each product was determined from the relative standard curves constructed with serial dilutions of the control cDNA.

Real-Time PCR Microarray Analysis

We isolated RNA from the hearts of WT and CHOP-deficient mice at 4 weeks after TAC or sham operation. Then, the synthesis of cDNA and comparison of relative gene expressions for 15 Bcl2 family members were performed with the RT² First Strand Kit and a mouse PCR array (Superarray Bioscience Corp, Frederick, Md). Samples from 3 sham-operated and 3 pressure-overloaded hearts at 4 weeks after operation were compared in WT and CHOP-deficient mice. The average cycle threshold (Ct) was calculated for each Bcl2 family gene and the housekeeping genes (GAPDH and actin), and the ΔCt ($Ct_{\text{Bcl2 family gene}} - Ct_{\text{average of GAPDH and actin}}$) was determined.[22] The values were expressed as the $2^{-\Delta Ct}$, and data of sham-operated and pressure-overloaded hearts were analyzed with $2^{-\Delta\Delta Ct}$ method.[22]

Immunoblotting Analysis

Immunoblotting analysis was performed as described previously.[19] The mitochondrial fraction was extracted from mouse hearts with a Mitochondria Extraction Kit (Imgenex Corp, San Diego, Calif) according to the manufacturer's protocol.

Apoptotic Cell Assay

The terminal deoxynucleotidyl transferase dUTP nick-end labeling (TUNEL) assay was performed as described previously.[9] The number of TUNEL-positive cells was expressed as a percentage of total cells.

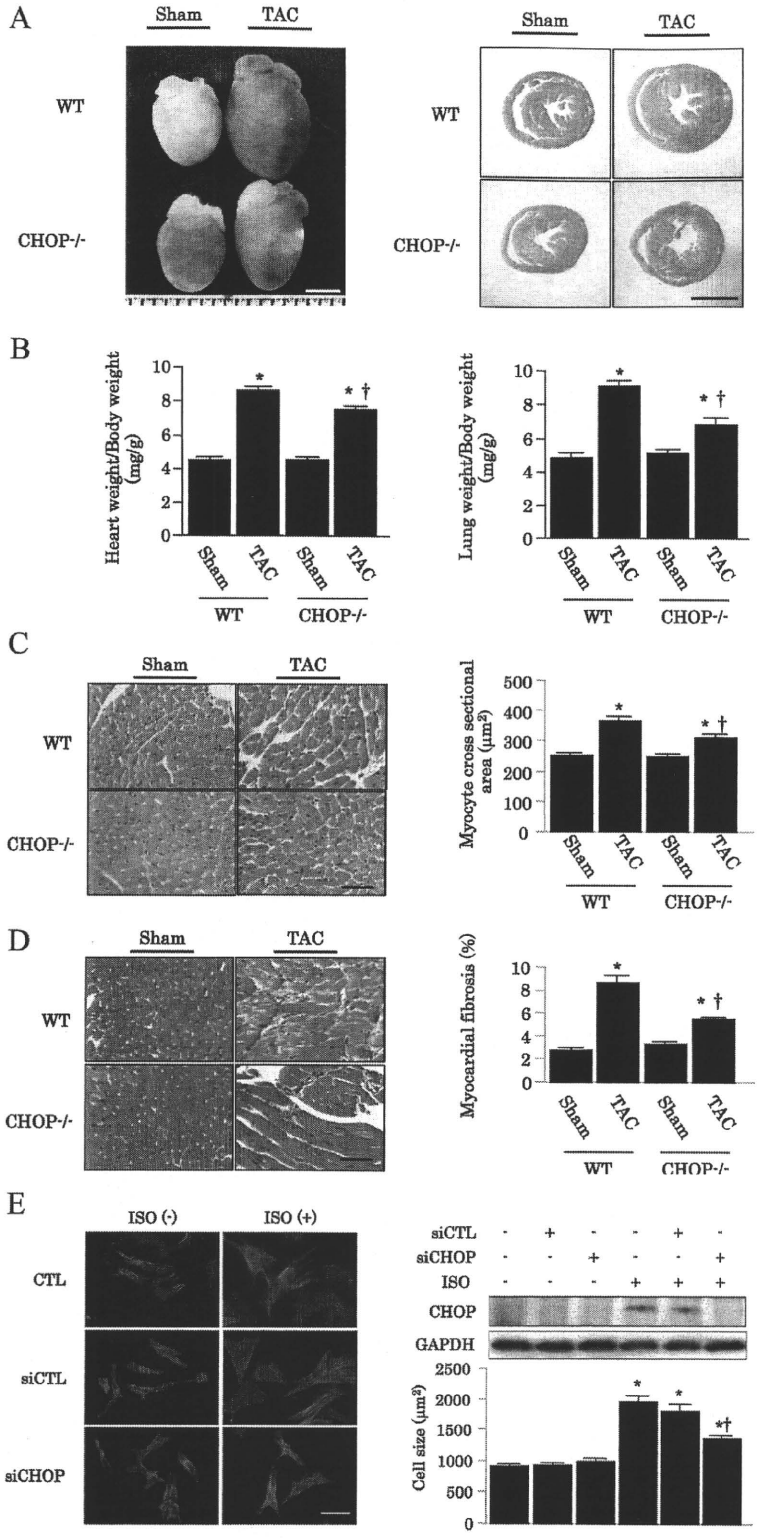

Figure 2. Attenuation of cardiac hypertrophy and dysfunction induced by pressure overload in CHOP-deficient mice. A, left, Representative gross appearance of hearts from WT and CHOP-deficient mice. Scale bars=2.5 mm. Right, Representative hematoxylin and eosin–stained cross sections of LV myocardium from WT and CHOP-deficient mice. Scale bars=2.5 mm. B, Ratios of heart weight to body weight (left) and lung weight to body weight (right) of WT mice (n=16) and CHOP-deficient mice (n=15). C, Representative pictures of myocardium with hematoxylin and eosin stain (left) and quantitative analysis of myocyte cross-sectional area (right). Bar=50 μm. D, Representative pictures of myocardium with Masson trichrome stain (left) and quantitative analysis of cardiac fibrosis (right). Bar=50 μm. *†$P<0.05$ vs WT mice at 4 weeks after sham operation and TAC, respectively. E, Representative pictures showing cultured rat neonatal cardiomyocytes stained with rhodamine-phalloidin (left), representative immunoblotting of CHOP (top right), and quantitative analysis of cell size (bottom right). Cardiomyocytes were treated with siRNA for CHOP (siCHOP) or firefly luciferase from Photinus pyralis (siCTL) as a negative control (60 nmol/L) 4 hours after cardiomyocyte isolation. The immunoblotting and histological analyses were performed 24 hours after treatment with isoproterenol (ISO; 10 μmol/L). *†$P<0.05$ vs control (CTL) and isoproterenol treatments, respectively.

versus 111±3 mm Hg), between WT mice and CHOP-deficient mice. On gross examination, CHOP-deficient mice showed less enlargement of the heart compared with WT mice at 4 weeks after TAC (Figure 2A). The ratios of heart weight to body and lung weight to body weight at 4 weeks after TAC were both significantly smaller in CHOP-deficient mice than in WT mice (Figure 2B). On microscopic examination, CHOP-deficient mice showed less cardiac hypertrophy (Figure 2C) and cardiac fibrosis (Figure 2D) compared with WT mice at 4 weeks after TAC. In cultured rat neonatal cardiomyocytes, the knockdown of *CHOP* by siRNA targeting *CHOP* decreased CHOP protein levels by 80% and significantly attenuated the increase in cell size in response to isoproterenol (Figure 2E).